Title

Mechanism and Kinetics of Acetone Conversion to Isobutene over Isolated Hf Sites Grafted to Silicalite-1 and SiO2

Journal

Journal of the American Chemical Society, 143(22)

ISSN

0002-7863

Authors

Zhang, Yanfei
Qi, Liang
Lund, Alicia
et al.

Publication Date

2021-06-09

DOI

10.1021/jacs.1c01315

Peer reviewed

JACS
JOURNAL OF THE AMERICAN CHEMICAL SOCIETY
pubs.acs.org/JACS
Article

Mechanism and Kinetics of Acetone Conversion to Isobutene over Isolated Hf Sites Grafted to Silicalite-1 and SiO_2

Yanfei Zhang, Liang Qi, Alicia Lund, Peng Lu, and Alexis T. Bell*

Cite This: J. Am. Chem. Soc. 2021, 143, 8352−8366
Read Online

ABSTRACT: Isolated hafnium (Hf) sites were prepared on Silicalite-1 and SiO_2 and investigated for acetone conversion to isobutene. Characterization by IR, ^{1}H MAS NMR, and UV−vis spectroscopy suggests that Hf atoms are bonded to the support via three O atoms and have one hydroxyl group, i.e, $(\equiv SiO)_3Hf-OH$. In the case of Hf/Silicalite-1, Hf−OH groups hydrogen bond with adjacent Si−OH to form $(\equiv SiO)_3Hf-OH\cdots HO-Si\equiv$ complexes. The turnover frequency for isobutene formation from acetone is 4.5 times faster over Hf/Silicalite-1 than Hf/SiO_2. Lewis acidic Hf sites promote the aldol condensation of acetone to produce mesityl oxide (MO), which is the precursor to isobutene. For Hf/SiO_2, both Hf sites and Si−OH groups are responsible for the decomposition of MO to isobutene and acetic acid, whereas for Hf/Silicalite-1, the $(\equiv SiO)_3Hf-OH\cdots HO-Si\equiv$ complex is the active site. Measured reaction kinetics show that the rate of isobutene formation over Hf/SiO_2 and Hf/Silicalite-1 is nearly second order in acetone partial pressure, suggesting that the rate-limiting step involves formation of the C−C bond between two acetone molecules. The rate expression for isobutene formation predicts a second order dependence in acetone partial pressure at low partial pressures and a decrease in order with increasing acetone partial pressure, in good agreement with experimental observation. The apparent activation energy for isobutene formation from acetone over Hf/SiO_2 is 116.3 kJ/mol, while that for Hf/Silicalite-1 is 79.5 kJ/mol. The lower activation energy for Hf/Silicalite-1 is attributed to enhanced adsorption of acetone and formation of a C−C bond favored by the H-bonding interaction between Hf−OH and an adjacent Si−OH group.

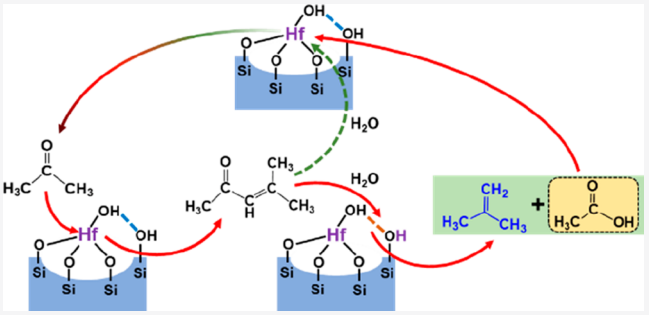

1. INTRODUCTION

Isobutene is an important chemical intermediate used to produce a broad range of products. These include octane blending components for gasoline (e.g., isooctane, methyl-*tert*-butyl ether (MTBE), and ethyl-*tert*-butyl ether (ETBE)), butyl rubber, methyl methacrylate, methacrolein, and acrylics.[1−5] The primary sources of isobutene today are steam cracking of naphtha, isomerization and dehydrogenation of petroleum-derived butane, and separation from the butane−butene fraction produced by catalytic cracking of petroleum.[5,6] However, growing concerns with global warming caused by the combustion of products derived from petroleum have motivated the search for routes to isobutene based on biomass as the starting material.[7−9] An attractive approach for doing so is the condensation of acetone, produced by the fermentation of glucose to a mixture of acetone, butanol, ethanol (so-called ABE fermentation) or the ketonization of acetic acid. If acetic acid produced as a byproduct of acetone condensation is converted back to acetone and CO_2, the overall reaction for the synthesis of isobutene from acetone is

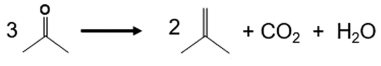

This reaction is thermodynamically favorable (ΔG°_{298} = −35 kJ/mol) and has a carbon utilization efficiency of 88.9%.

Previous investigations of acetone condensation to isobutene have focused on the use of Brønsted acid zeolites, e.g., SAPO-34, H-MFI and H-BEA, as the catalyst. These studies suggest that isobutene is formed by successive aldol condensation and self-deoxygenation.[10−13] While Brønsted acidic zeolites are demonstrated to be very active for acetone conversion to isobutene, low isobutene selectivity and rapid catalyst deactivation due to coking have discouraged their further development.

The use of Lewis acid sites have been examined by a number of investigators for reactions involving the formation of C−C bonds via aldol condensation.[14−17] Román-Leshkov et al. have reported Hf-, Sn-, and Zr-BEA to be active for the cross-aldol condensation of aromatic aldehydes and acetone.[18] Li and

Received: February 3, 2021
Published: May 27, 2021

https://doi.org/10.1021/jacs.1c01315
J. Am. Chem. Soc. 2021, 143, 8352−8366

coworkers have reported that 10 wt % Y/BEA (YO_x supported on dealuminated BEA zeolite (DeAlBEA)) is an effective catalyst for acetic acid conversion to isobutene with 100% conversion and 60% isobutene selectivity.[15] Lewis acid sites have also been proposed as aldol condensation centers for producing C_6 intermediates over Y_2O_3 and YO_x species supported on DeAlBEA. More recently, Shylesh et al. have demonstrated C−C bond formation via propanoic acid ketonization and acetone aldol condensation to mesityl oxide (MO) over site-isolated Zr catalyst (Zr/SiO_2) containing ≡Zr−OH sites.[19]

Previous studies have also found that the local environment of Lewis acidic metal centers influence their catalytic performance. For the reaction of acetone to isobutene, Li et al. found that the catalytic efficiency of Y/SiO_2 was much lower than that of Y/DeAlBEA, and Y/Silicalite-1 showed almost no C−C coupling activity. This much lower activity was ascribed to the weaker interaction of Y species with SiO_2 and Silicalite-1 compared with DeAlBEA.[15]

Here, we describe the preparation of isolated Lewis acidic Hf sites on SiO_2 and Silicalite-1. Hf was chosen for these studies rather than Zr or Y for the following reasons.[18,20,21] The Lewis acidity of Hf is slightly lower than that of Zr, which should result in a higher isobutene selectivity without significant sacrifice in activity,[20,21] and compared to Y, Hf grafted on silica and Silicalite-1 is expected to exhibit higher activity for aldol condensation.[15,22,23] The catalysts were characterized by XRD, IR, ^{1}H MAS NMR and UV−vis spectroscopy. The structure of the active Hf sites is proposed to be $(\equiv Si-O)_3-Hf-OH$ for both Hf/SiO_2 and Hf/Silicalite-1. In addition, for Hf/Silicalite-1, the Hf−OH groups H-bond with adjacent Si−OH groups. The influence of active site structure and local environment was investigated for the conversion of acetone to isobutene for both Hf/SiO_2 and Hf/Silicalite-1. The rate of isobutene formation on Hf/Silicalite-1 was found to be 4.5 times higher than that on Hf/SiO_2. The reactions of the intermediates involved in the conversion of acetone to isobutene−diacetone alcohol (DAA), mesityl oxide (MO), and acetic acid were also investigated with the aim of identifying the roles of these species in the overall reaction pathway. The accumulated information was used to propose a reaction mechanism for the conversion of acetone to isobutene over isolated Hf sites.

2. EXPERIMENTAL SECTION

2.1. Catalyst Preparation. *Preparation of Hf Grafted Silicalite-1 and SiO_2.* The silica support (SiO_2) was provided by Silicycle. Nanosheet-like Silicalite-1 (self-pillared pentasil) was synthesized following a modification of a method reported previously by Zhang et al.[24] Tetra(*n*-butyl) phosphonium hydroxide (TBPOH) (Sigma-Aldrich, 40%) and fumed silica (Sigma-Aldrich) were used as the structure-directing agent and silicon source, respectively. After crystallization, the as-synthesized material was washed with distilled water until the pH of the supernatant was lower than 9; the precipitate was then dried at 343 K in vacuum overnight and calcined at 823 K for 6 h in a muffle oven. To ensure complete removal of the residual organic structure-directing agent and decomposed organic moieties, the calcined material was washed twice with a large amount of deionized water at room temperature until the pH of the supernatant was close to 7, then dried at 343 K overnight, and calcined at 823 K for 6 h.[25]

Hafnium (Hf) was grafted onto Silicalite-1 and mesoporous SiO_2 by aqueous impregnation. Prior to introducing Hf, both supports, SiO_2 and Silicalite-1, were dehydrated at 353 K for 6 h in a vacuum drying oven and then stored in vacuum. Afterward, Hf was introduced on SiO_2 and Silicalite-1 by impregnating the support with aqueous solution of $HfCl_4$ with the Hf concentration adjusted to achieve the desired metal loadings. Typically, 2 mL of the $HfCl_4$ solution was used per gram of support. After impregnation, the slurry was dried in air at room temperature for 5 h, then heated to 323 K under flowing He, and held at this temperature for 2 h. This step was followed by further calcination in a muffle oven. The sample was heated from room temperature to 393 K over a 30 min period, then heated to 823 at 5 K min^{-1} and held at this temperature for 6 h, and finally cooled to room temperature. The samples prepared are designated as xHf/SiO_2 or xHf/Silicalite-1, respectively, where x designates the surface concentration of Hf (atoms nm^{-2}).

2.2. Catalyst Characterization. Powder X-ray diffraction (XRD) patterns of Silicalite-1 and Hf supported catalysts were recorded using a Bruker D8 GADDS diffractometer equipped with a Cu Kα target (40 kV and 40 mA) X-ray source. To observe the morphologies of Silicalite-1, scanning electron microscopy (SEM) images were acquired using a Thermo Scientific Helios G4 UC Focused Ion Dual Beam microscope operated with an accelerating voltage of 2 kV and a probe current of 25pA using a TLD detector. The specific surface areas of all samples were determined by acquiring N_2 adsorption isotherms at 77 K with a Micrometrics Gemini VII 2390 analyzer. The total surface areas were evaluated by applying the Brunauer−Emmet−Teller (BET) equation. Prior to analysis, samples were degassed for 6 h at 453 K. The Hf loadings were analyzed with inductively coupled plasma optical emission spectroscopy (ICP-OES) by Galbraith Laboratories, Inc.

Fourier transform infrared (FTIR) spectra were collected to characterize surface hydroxyl groups using a Thermo Scientific Nicolet 6700 IR spectrometer equipped with a liquid N_2-cooled MCT detector. Samples (~36 mg) were pressed into thin self-supporting wafers and then transferred to a transmission IR cell equipped with CaF_2 windows. Prior to the acquisition of spectra, samples were pretreated under dry flowing air (Praxair, ultrazero, 100 mL min^{-1}) for 1 h at 773 K to remove impurities and moisture and then cooled to 393 K. Spectra were recorded at 393 K with a resolution of 1 cm^{-1} and an accumulation of 64 scans.

The acid properties of Hf/SiO_2 and Hf/Silicalite-1 were characterized by FTIR spectroscopy of adsorbed pyridine using a Thermo Scientific Nicolet 6700 IR spectrometer. Prior to the acquisition of spectra, samples were pretreated at 773 K for 1 h in a flow of 100 mL min^{-1} air and then cooled to 393 K to take background scans. FTIR spectra of adsorbed pyridine were recorded by injecting 2 μL of pyridine and then purging the IR cell with He at 393 K for 20 min to remove any physically adsorbed material.

FTIR spectra were collected at a resolution of 4 cm^{-1} during the reaction of acetone as well as mesityl oxide (MO) over Hf/Silicalite-1. For these experiments, 30 mg of sample was pressed into a thin self-supporting wafer, transferred into the transmission IR cell, and pretreated at 773 K for 1 h in 100 mL min^{-1} of dry air. Subsequently, the sample was purged with 30 mL min^{-1} of He (Praxair, UHP) and cooled to 306 K to collect the background spectrum. After that, 2 μL of acetone was fed onto the catalyst under flowing He (Praxair, UHP, 30 mL min^{-1}), and the spectra were recorded at constant time intervals. For the reaction of MO, 0.2 μL MO was injected under similar reaction conditions.

Prior to carrying out the NMR experiment, all samples were dehydrated overnight at 353 K under vacuum, and then the material was packed in a 4 mm zirconia rotor inside the glovebox. The rotor was then placed inside a Bruker high resolution dual resonance ^{1}H/^{13}C magic angle spinning (MAS) probe that has a ^{1}H frequency of 500 MHz. All NMR measurements were recorded with a spinning rate of 10 kHz. The quantitative ^{1}H spectra were acquired using the DEPTH pulse sequence with a recycle delay of 2 s,[26] equivalent to five times the spin−lattice T_1 relaxation, and a radio frequency power of 80 kHz. The spectra were fitted with Dmfit software.[27]

Ultraviolet−visible (UV−vis) diffuse reflectance spectra of Silicalite-1, SiO_2, and Hf supported samples are collected with a Fischer Scientific Evolution 300 spectrometer equipped with a Harrick Scientific Praying Mantis diffuse reflectance chamber. Samples were grounded and dehydrated at 473 K for 20 min in a

https://doi.org/10.1021/jacs.1c01315
J. Am. Chem. Soc. 2021, 143, 8352−8366

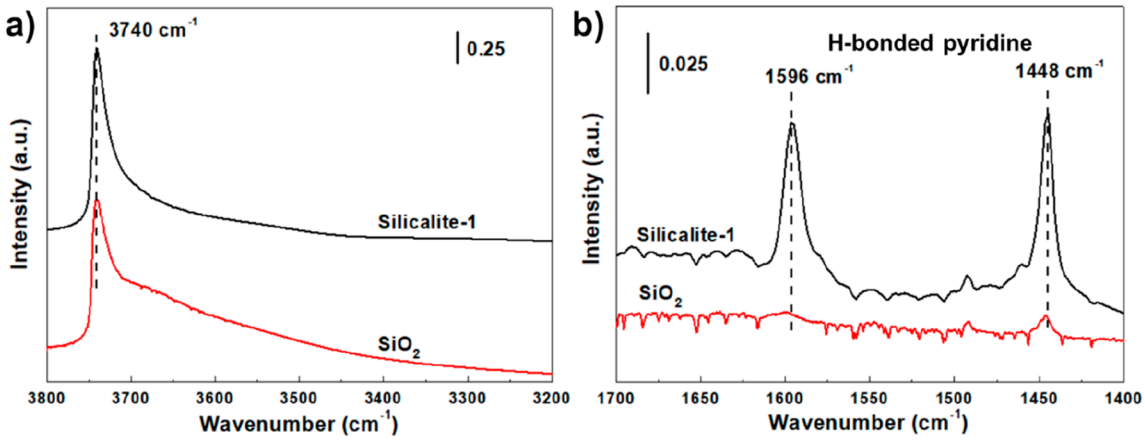

Figure 1. (a) FTIR spectra for the hydroxyl stretching region and (b) FTIR spectra following pyridine adsorption of Silicalite-1 and SiO_2.

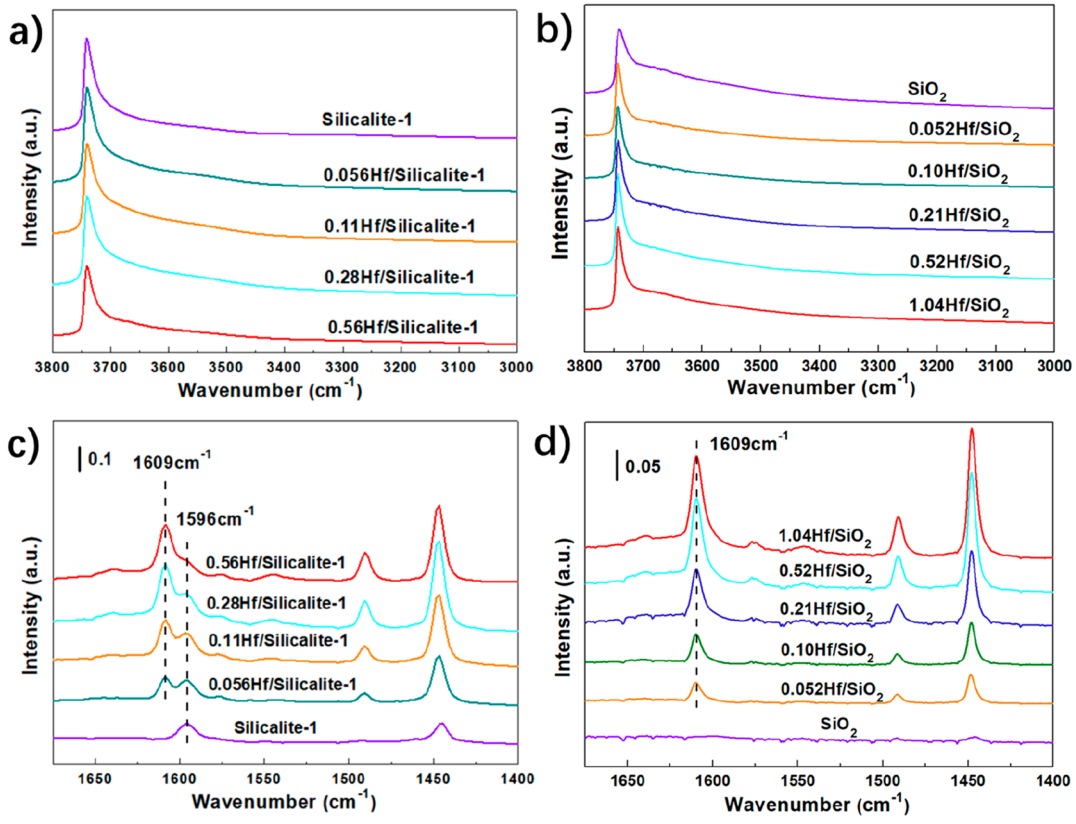

Figure 2. Effect of Hf loading on the FTIR spectra of surface hydroxyl groups and FTIR spectra taken following pyridine adsorption on (a, c) Hf/Silicalite-1 and (b, d) Hf/SiO_2.

flow of 120 mL min^{-1} air and then cooled to 303 K to collect spectra. Dehydrated $BaSO_4$ was used as a reference.

2.3. Catalyst Evaluation. Catalyst performance was evaluated at atmospheric pressure using a 6.35 mm OD quartz reactor, whereas reaction kinetics were determined using a 6.35 mm OD quartz tube with an expanded section (~12.7 mm OD). Quartz wool was placed below the catalyst bed to hold the catalyst in place, and a thermocouple was fixed at the center of catalyst bed. Prior to initiating reaction, each catalyst was pretreated in flowing air (Praxair, ultrazero, 30 mL min^{-1}) at 823 K for 40 min and then cooled to reaction temperature and purged with He (Praxair, 99.999%, 20 mL min^{-1}) for 10 min. All chemicals were obtained commercially and used without further purification. Acetone (≥99.9%), 4-hydroxy-4-methyl-2-pentanone (diacetone alcohol, 99%), and acetic acid (>99%) were obtained from Sigma-Aldrich. Mesityl oxide (90%, remainder 4-methyl-4-penten-2-one) was purchased from Alfa Aesar.

Reactions were performed using He as the carrier gas. In a typical run, a syringe pump (KD Scientific, Legato 100 series, <5% fluctuation) was used to supply liquid-phase reactants (i.e., acetone, acetone-H_2O mixture, diacetone alcohol−H_2O mixture, mesityl oxide, and nanopure H_2O) into a heated port through which He flowed continuously. The product stream was analyzed using an Agilent 6890A gas chromatography (GC) equipped with a HP-5 capillary column, an FID, and a liquid N_2 cooling system.

In the exploration of the effect of water partial pressure on the rate of isobutene formation from acetone, a constant acetone partial pressure of 1 kPa was cofed with water partial pressure ranging from 20 to 3 kPa, corresponding to steam-to-carbon (S/C) ratios of 6.67 to 1. For each combination of acetone/H_2O, the rate of isobutene

https://doi.org/10.1021/jacs.1c01315
J. Am. Chem. Soc. 2021, 143, 8352−8366

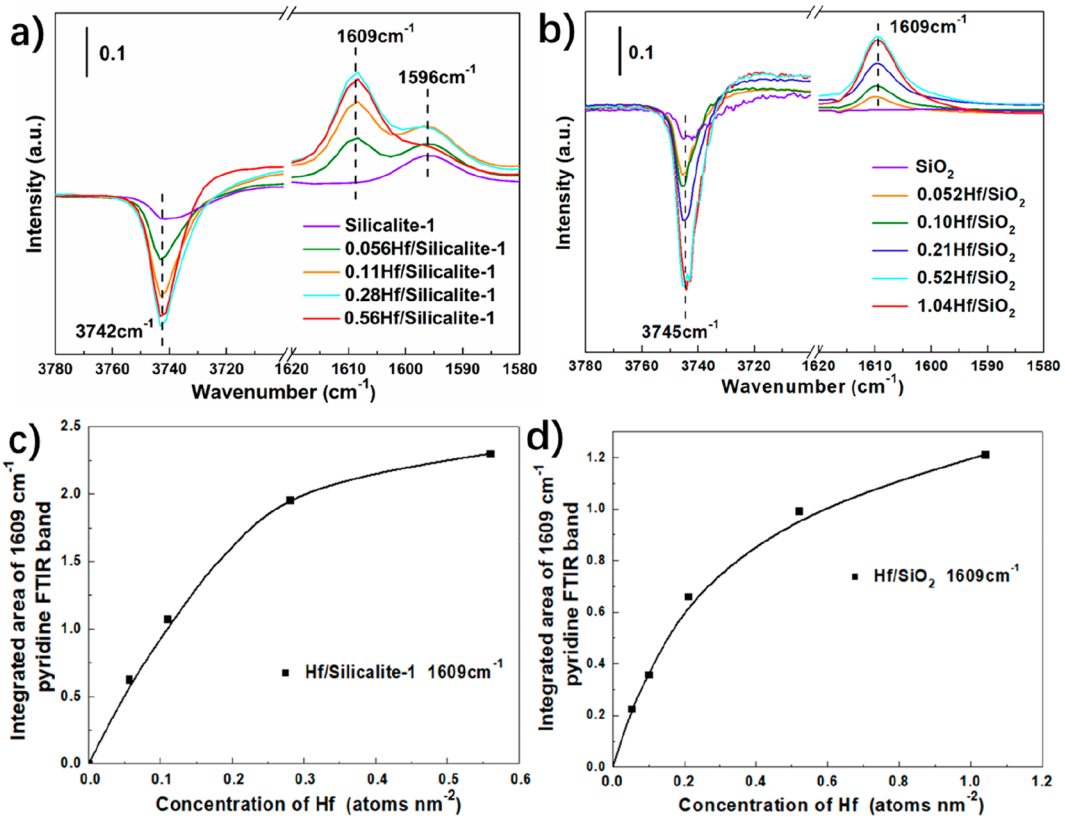

Figure 3. Difference spectra obtained by subtracting the spectrum of the catalyst prior to pyridine adsorption from that taken after pyridine adsorption for (a) Hf/Silicalite-1 and (b) Hf/SiO_2 for different Hf loadings. Plots of the integrated area for the band at 1609 cm^{-1} versus Hf loading for (c) Hf/Silicalite-1 and (d) Hf/SiO_2.

formation was measured after cofeeding acetone and water for 5 min. The rate of isobutene formation at 20 kPa of water partial pressure was then measured again to assess whether catalyst deactivation had occurred. No catalyst deactivation was detected in these experiments.

3. RESULTS AND DISCUSSION

3.1. Catalyst Characterization. XRD patterns of Silicalite-1 as well as Hf/Silicalite-1 with different Hf loadings are shown in Figure S1; Hf/Silicalite-1 exhibit characteristic peaks at 2θ = 7−10° and 22−25° of MFI zeolites and no obvious peaks representing HfO_2 for Hf concentration up to 0.56 Hf atoms nm^{-2}, indicating high dispersion of Hf. The elemental composition of each sample was analyzed by ICP-OES and are summarized in Table S1. The weight loadings of Hf detected closely match the intended metal loadings, confirming the successful introduction of the metal. Preservation of the crystalline structure Silicalite-1 was further confirmed by the N_2 adsorption; only a slight decrease in the BET surface area and volume were observed for Hf/Silicalite-1 with Hf concentration ranging from 0.056 to 0.56 Hf atoms nm^{-2}. Additionally, as shown in Table S1, the BET surface area of Silicalite-1 is 603 $m^2\ g^{-1}$, almost twice the value of SiO_2 (323 $m^2\ g^{-1}$), consistent with its nanosheet-like morphology (Figure S2).

FTIR spectroscopy was used to characterize the surface O−H groups of Silicalite-1 and SiO_2. As seen in Figure 1a, both Silicalite-1 and SiO_2 show a signal at around 3740 cm^{-1} attributable to isolated Si−OH groups.[28] After pyridine adsorption, two strong signals appear at 1596 and 1448 cm^{-1} on Silicalite-1 that can be ascribed to hydrogen (H)-bonded pyridine.[29,30] By contrast, almost no signal is observed for pyridine interaction with SiO_2. This suggests that the acidity of silanol groups on SiO_2 is weaker than those on Silicalite-1.

Hf/Silicalite-1 and Hf/SiO_2 samples with different Hf loadings were also characterized by FTIR. As shown in Figure 2a and b, a slight intensification of the band at 3740 cm^{-1} for isolated Si−OH groups was observed for both sets of samples. This phenomenon is unexpected considering the consumption of Si−OH groups during the introduction of Hf species. A plausible explanation for this observation is that Hf−OH groups exhibit a peak at a similar position as that for isolated Si−OH groups.[31]

FTIR spectra of pyridine adsorbed on Hf/Silicalite-1 and Hf/SiO_2 are shown at Figure 2c and d. For Hf/Silicalite-1, a band for pyridine interactions with Lewis acid centers and a second band for pyridine interactions with both Brønsted and Lewis acid centers are observed at 1609 and 1490 cm^{-1}, respectively.[30] The intensity of these three bands increases with increasing Hf loading up to a loading of 0.28 Hf atoms nm^{-2}. It is also notable that the integrated intensity of the band for H-bonded pyridine at 1596 cm^{-1} increases monotonically with Hf concentration on Silicalite-1 up to a Hf concentration of 0.28 Hf atoms nm^{-2} (see Figure S3). Although Hf grafting consumes H-bonded Si−OH groups and, hence, is expected to decrease intensity of the signal at 1596 cm^{-1}, the interaction between newly generated Hf−OH group and residual Si−OH groups leads to the intensification of this band; additional evidence for this process is presented in Figures 3 and 4. For Hf/SiO_2, very similar bands are observed at 1448, 1490, and 1609 cm^{-1} after pyridine adsorption, and the intensity of these

https://doi.org/10.1021/jacs.1c01315
J. Am. Chem. Soc. 2021, 143, 8352−8366

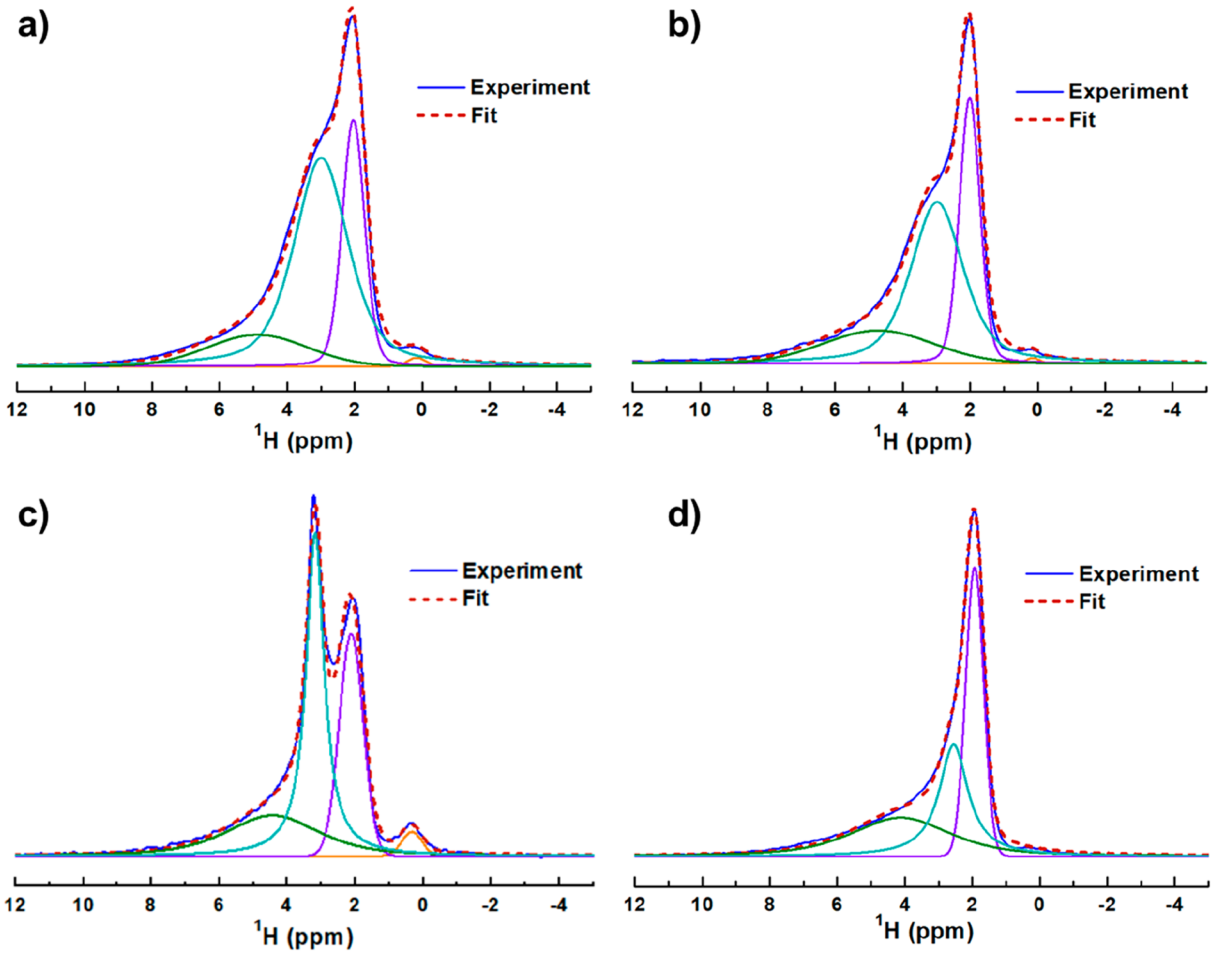

Figure 4. ^{1}H MAS NMR spectra of (a) SiO_2, (b) 0.21Hf/SiO_2, (c) Silicalite-1, and (d) 0.28Hf/Silicalite-1. Prior to acquiring NMR spectra, each sample was dehydrated at 353 K under vacuum.

three bands increases with increasing Hf concentration below 0.52 Hf atoms nm^{-2}. In sharp contrast to what is observed on Silicalite-1, no bands for H-bonded pyridine were detected over Hf/SiO_2 despite the observation of Hf-OH groups in Figure 3b. Moreover, as shown in Figure S4, the intensity of the band for pyridine interacting with Lewis acid centers on Hf/SiO_2 is weaker than that for Hf/Silicalite-1 containing the same number of moles of Hf. Accordingly, Lewis acidic sites are generated via the introduction of Hf. In addition, the intensification of band at 1596 cm^{-1} for Hf/Silicalite-1 with increasing Hf contents suggests that H-bonding interaction of Hf-OH with Si-OH groups is presented.

The integrated areas of the band at 1609 cm^{-1} for Hf/Silicalite-1 and Hf/SiO_2 are plotted in Figure 3 against the surface concentration of Hf. The integrated peak areas are normalized by the intensity of the bands for Si−O−Si framework overtones appearing between 1700−2000 cm^{-1}.[32] As seen in Figure 3c, the area of the band at 1609 cm^{-1} for Hf/Silicalite-1 increases linearly up to a Hf concentration of 0.28 Hf atoms nm^{-2}, suggesting the generation of isolated Hf Lewis acid centers in this range. Above 0.28 Hf atoms nm^{-2}, the rate of increase in intensity decreases, due to the possible generation of hafnium oxide oligomers and/or nanoclusters. A similar linear increase in the intensity of the band at 1609 cm^{-1} is also observed for Hf/SiO_2 for Hf concentrations below 0.21 Hf atoms nm^{-2} (Figure 3d), which also indicates isolated Hf sites are present. However, as noted before, the integrated area of the band at 1609 cm^{-1} for Hf/Silicalite-1 is always larger than that for Hf/SiO_2 for the same molar concentration of Hf.

Another interesting feature of the IR spectra of adsorbed pyridine is the negative band for hydroxyl vibrations. This feature in Figure 3a and b provides direct evidence for the interaction of pyridine with hydroxyl groups, either Si−OH and/or Hf−OH. The negative peaks are centered at 3742 and 3745 cm^{-1} for Hf/Silicalite-1 and Hf/SiO_2, respectively. For both samples (Figure S5), the integrated negative peak areas increase linearly with Hf concentration from 0.056 to 0.28 Hf atoms nm^{-2} for Hf/Silicalite-1, and with Hf concentration between 0.052 and 0.21 Hf atoms nm^{-2} for Hf/SiO_2, consistent with the linear increase of 1609 cm^{-1} bands. Such negative peaks are much weaker for either Silicalite-1 or SiO_2 because of the weaker interaction between silanol and pyridine compared with Hf−OH. It has been reported that Zr grafted on SiO_2 and the open Sn sites on dealuminated beta both have M−OH groups. IR spectra of ZrO_2 or ZrO_x supported on siliceous materials exhibits Zr−OH bands at 3740−3775 cm^{-1}.[31,33,34] Although no information has been reported for Hf−OH, considering the similarity of the electronic structures and Lewis acid property of Zr and Hf,[18] it is reasonable to expect Hf−OH signals in a similar range to those found for Zr−OH. As a result, the negative peak is proposed to be associated with either Hf−OH itself or with Hf−OH H-bonded to an adjacent Si−OH. The existence of the latter

https://doi.org/10.1021/jacs.1c01315
J. Am. Chem. Soc. 2021, 143, 8352−8366

complex is suggested by the observation of H-bonded pyridine signals at 1596 cm^{-1}. For Hf/SiO_2, the negative hydroxyl peak is attributed to the interaction of pyridine with Hf-OH groups because no signal of pyridine interacting with Hf-OH H-bonded to an adjacent Si-OH group was observed. By contrast, for Hf/Silicalite-1, the observation of H-bonded pyridine and the broader negative hydroxyl peak both suggest that this peak is most likely attributable to the interaction of pyridine with both Hf−OH and Si−OH groups. Based upon the linear enhancement of the band for pyridine interaction with Lewis acid sites and with the −OH groups of Hf−OH for both Hf/Silicalite-1 and Hf/SiO_2, we propose that isolated Hf sites with structure of $(\equiv SiO)_3$−Hf−OH are formed over SiO_2 and Silicalite-1. This interpretation is fully consistent with many previous studies of supported, isolated Lewis acidic sites.[19,35−38] Such sites have two chemical structures, i.e., closed ($(\equiv SiO)_4$−M) and open ($(\equiv SiO)_3$−M−OH) sites. Open sites with relatively stronger Lewis acidity are found to be more active for aldol condensation with respect to closed sites.[36,39]

^{1}H MAS NMR spectroscopy was used to further characterize the hydroxyl groups on SiO_2, Silicalite-1, and Hf supported on both siliceous supports. All NMR spectra were deconvoluted by fitting them with Dmfit software to distinguish the overlapping peaks. As shown in Figure 4a and c, after deconvolution, four similar peaks can be identified for both SiO_2 and Silicalite-1. The ^{1}H MAS NMR spectrum of SiO_2 shows signals at 0.16, 2.1, 3.0, and 4.6 ppm. The peaks at 2.1 and 3.0 ppm are assigned to isolated silanol groups and weakly H-bonded Si−OH groups, respectively, while the peak at 4.6 ppm is due to clusters of adsorbed H_2O.[40−44] The very small peak at 0.16 ppm is probably due to some impurity species. Similar peaks for isolated and H-bonded Si−OH groups are detected for Silicalite-1 at around 2.1 and 3.2 ppm, respectively.[40,45,46] A signal representative of bulk H_2O adsorbed on Si−OH groups is also detected at 4.4 ppm.[43] The line width of the signal for H-bonded Si−OH for Silicalite-1 is much narrower than that for SiO_2 (0.64 vs 1.8), which suggests a relatively uniform distribution of H-bonded Si−OH groups on the former support. The larger chemical shift for H-bonded Si−OH groups observed for Silicalite-1 compared to SiO_2 is evidence for stronger H-bonding interaction between Si−OH groups on Silicalite-1.

The assignment of ^{1}H NMR signals for grafted Hf−OH groups has not been reported previously. Therefore, we looked for analogies with the assignment of Zr−OH groups because Zr and Hf are both d-block transition metals with similar electronic structures. The ^{1}H MAS NMR peak observed at 1.8 ppm for ZrO_xH_y aerogels has been assigned to terminal Zr−OH groups.[47] Similarly, it has been reported that the ^{1}H MAS NMR signal shifts from 1.5 to 1.7 ppm upon incorporation of Zr into dealuminated BEA.[48] In another example, it has been reported that the ^{1}H MAS NMR chemical shift of terminal Zr hydroxyl groups appears at either 1.6 or 1.8 ppm.[49] Accordingly, the ^{1}H MAS NMR signal of Hf−OH is proposed to be located between 1.6 and 2.0 ppm, a position similar to that for isolated Si−OH groups. For Hf/SiO_2, the ^{1}H signal is located at 2.0 ppm. By comparison, the ^{1}H chemical shift for SiO_2 is 2.1 ppm. We note as well that the intensity of this signal increases after grafting Hf. As discussed above, the chemical shift at 2.0 ppm for Hf/SiO_2 could have contributions from both Hf−OH groups and residual terminal Si−OH groups because the chemical shifts for Si−OH and Hf−OH groups are very similar.

We note further that the position of the signal for Si−OH groups H-bonding with Hf−OH groups in Hf/Silicalite-1 is 2.6 ppm and has a line width of 1.0 ppm compared to that for non-H-bonded Si−OH groups which is positioned at 3.2 ppm and has a line width of 0.64 ppm. These features for Si−OH groups H-bonding with Hf−OH groups are absent from the NMR spectrum of Hf/SiO_2. Together with the intensification of H-bonded pyridine signal observed upon introducing Hf to Silicalite-1 (Figures 2c and S3), the broadened H-bonded proton signal at 2.6 ppm observed for Hf/Silicalite-1 is attributed to H-bonding between the hydroxyl group Hf−OH and an adjacent Si−OH group.

The data reported in Figures 4c and d and Figure S6b and Tables S2−S5 were used to evaluate the assumption that Hf is bonded to Silicalite-1 via three Si−O−Hf bonds (i.e., $(\equiv Si-O-)_3$Hf−OH). This assessment begins with recognizing that Silicalite-1 has 3.77 Si−OH groups nm^{-2} on its surface based on deconvolution of ^{29}Si NMR spectra.[25] The data in Table S2 indicate that 62% of these silanol groups are H-bonded, and 38% are isolated silanol groups. Only the H-bonded silanol groups are expected to be active in forming $(\equiv SiO)_3$Hf−OH groups, which means that grafting Hf to obtain a loading of 0.24 Hf atoms nm^{-2} (determined by ICP for 0.28Hf/Silicalite-1) will consume 0.72 Si−OH nm^{-2}, or 31% of the original inventory of H-bonded silanol groups, 2.34 Si−OH nm^{-2}. This calculation suggests that the intensity of the peak at 2.6−3.2 ppm in the ^{1}H NMR spectrum of 0.28Hf/Silicalite-1 should decrease by 31% relative to that in the spectrum of Silicalite-1. However, this projection does not recognize that the ^{1}H NMR shift for the Hf−OH group is virtually the same as that for the Si−OH group. Taking this into account means that the projected decrease in the intensity of the ^{1}H NMR peak at 2.6−3.2 ppm should be 20.5%. The latter figure agrees reasonably well with the observed decrease of 21.8%. A similar calculation made for 0.21Hf/SiO_2 (see the Supporting Information for details) predicts that the peak at 3.0 ppm should decrease by 15.6%. While this value is much larger than that observed, 5.8%, it is still qualitatively consistent. The consumption of H-bonded silanol groups upon grafting Hf onto SiO_2 is also evidenced by the loss of intensity in the broad band located between 3710 and 3400 cm^{-1}, which shows a decrease in intensity of about 18.8% upon the introduction of 0.18 Hf atoms nm^{-2} (measured by ICP for 0.21Hf/SiO_2 sample), in better agreement with what is predicted.

We would like to note that the ^{1}H NMR signal for H-bonded −OH groups decreases in intensity after Hf is grafted onto Silicalite-1. This pattern appears to contradict the trends seen in the IR spectra of pyridine adsorbed on Silicalite-1 and Hf/Silicalite-1 (shown in Figures 2c and S3). These spectra show that the band at 1596 cm^{-1} for H-bonded pyridine increases monotonically with Hf concentrations up to 0.28 Hf atoms nm^{-2}. We believe that this apparent discrepancy is attributable to the higher IR extinction coefficient for pyridine interacting with the more acidic H-bonded Hf−OH groups than Si−OH groups.[50,51] This difference compensates the decrease in intensity of the IR signal for pyridine H-bonded to Si−OH groups. This interpretation is consistent with our deduction that three Si−OH groups are consumed for each Hf grafted; hence, the intensity of ^{1}H NMR signal of H-bonded −OH groups decreases after the introduction of Hf due to the decrease of proton density.

https://doi.org/10.1021/jacs.1c01315
J. Am. Chem. Soc. 2021, 143, 8352−8366

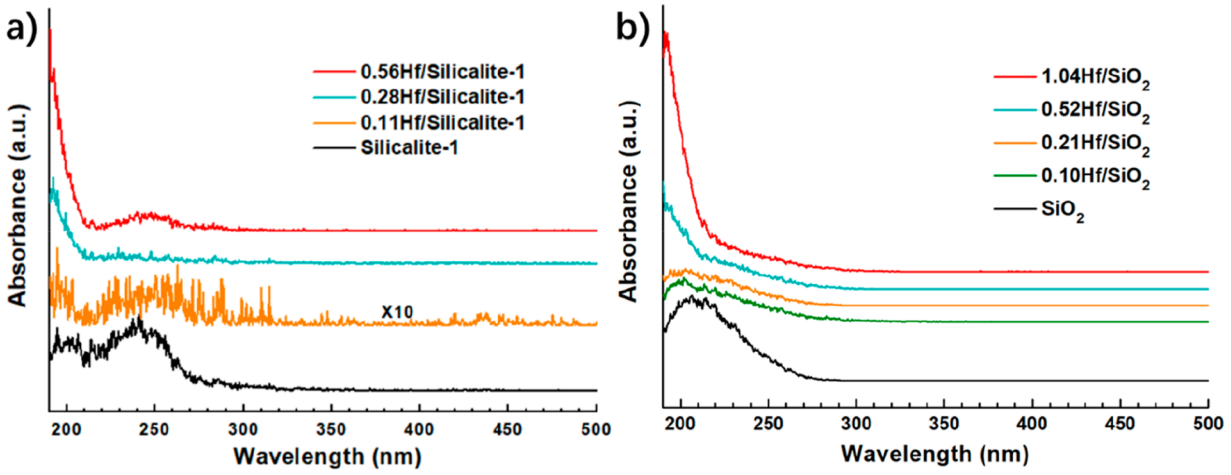

Figure 5. Effect of Hf concentration on the UV−vis spectra of (a) Hf/Silicalite-1 and (b) Hf/SiO_2.

Figure 5 presents UV−vis spectra for SiO_2, Silicalite-1, and Hf supported samples. Silicalite-1 exhibits two absorption peaks at ca. 200 and 240 nm, respectively, whereas SiO_2 exhibits a broad absorption peak between 190 and 270 nm. These features are attributable to the presence of Si−OH groups.[52,53] After grafting Hf, the absorption peaks ascribed to Si−OH groups in Silicalite-1 and SiO_2 lose intensity due to their consumption upon introduction of Hf, consistent with what is observed by FTIR and ^{1}H NMR spectroscopy. It should be noted that although the absorption signal for 0.11Hf/Silicalite-1 is weak due to the low concentration of grafted Hf, the absorption in the low wavelength region (below 210 nm) becomes evident when Hf loading rises to 0.28 atoms nm^{-2}. This feature can be attributed to the introduction of isolated Hf species. The absorption becomes stronger when the Hf loading increases to 0.56Hf atoms nm^{-2}, at which point another broad absorption appears at 220−260 nm, which may be due to the presence of HfOx clusters.[54] For Hf/SiO_2, signal overlap between SiO_2 support and Hf occurs when the Hf concentrations is below 0.21 Hf atoms nm^{-2}. However, a shift of the absorption peak from high to low wavelength is still observed as the Hf loading increases from 0 to 0.1 and then to 0.21 Hf atoms nm^{-2}. The absorption peak becomes prominent at an Hf concentration of 0.52 Hf atoms nm^{-2} and further intensifies for 1.04 Hf atoms nm^{-2}. The photon absorption energies for Hf/Silicalite-1 and Hf/SiO_2 attributable to ligand-to-metal charge transfer (LMCT) from O to an isolated Hf(IV) are estimated to be around 5.8 and 5.4 eV, respectively, much higher than that for bulk HfO_2, 4.4 eV.[55,56]

In summary, based on the information obtained from IR, the ^{1}H MAS NMR, and the UV−vis spectroscopy of Hf/SiO_2 and Hf/Silicalite-1, we propose that isolated Hf sites on SiO_2 and Silicalite-1 are bonded to three O atoms of the support and one −OH group as shown in Scheme 1. These structures are similar to those proposed previously for isolated Zr dispersed on siliceous supports and characterized by EXAFS, in addition to the techniques used in this study.[56,57] We note that for Hf/Silicalite-1, the Hf−OH groups are H-bonded to adjacent Si−OH groups.

3.2. Acetone Conversion to Isobutene. The reaction of acetone to isobutene over Hf/Silicalite-1 and Hf/SiO_2 was conducted under differential reaction conditions (acetone conversion <9%). Water was cofed with acetone at a steam-to-carbon (S/C) molar ratio of 5 to alleviate the deactivation of the catalyst.[5] For all of these experiments, isobutene was the dominant product with a carbon selectivity of about 85%, corresponding to 95% of the theoretical selectivity (88.9% on a carbon basis). It is noted that under similar reaction conditions, no products were observed for either SiO_2 or Silicalite-1.

Scheme 1. Chemical Structure of Hf Isolated Sites in (a) Hf/SiO_2 and (b) Hf/Silicalite-1

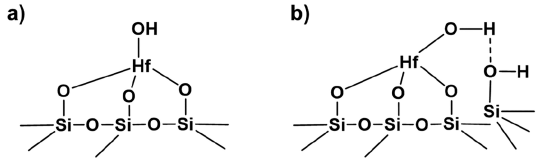

Figure 6 shows the rates of isobutene formation over Hf/SiO_2 and Hf/Silicalite-1 as a function of the surface concentration of Hf. The rate of isobutene formation per gram of catalyst increases linearly with Hf content for Hf/Silicalite-1 up to a Hf concentration of 0.28 Hf atoms nm^{-2}, after which it increases but at a much lower rate. Hf/SiO_2 exhibits a similar linear increase in isobutene formation rate with Hf content up to 0.21 Hf atoms nm^{-2} (inset in Figure 6a). The rates of isobutene formation normalized per Hf atom, the turnover frequency (TOF), are shown in Figure 6b. The TOF for Hf/Silicalite-1 is nearly independent of the Hf concentration up to 0.28 Hf atoms nm^{-2}, and for Hf/SiO_2, the TOF is constant for Hf concentration up to 0.21 Hf atoms nm^{-2}. The TOF suggests that isolated Hf active sites are created over both supports. It is also notable that the TOF for isobutene formation over Hf/Silicalite-1 is about 4.5 times of Hf/SiO_2. Considering the similar structure of Hf sites on these two supports, we attribute this significant difference to differences in the local environment of the isolated Hf sites. We note that our observations differ from those reported by Li et al., who observed mild activity over YO_x/SiO_2 but no activity over YO_x/Silicalite-1 for the reaction of acetic acid to isobutene.[15] While acetic acid was completely converted to acetone, no further aldol condensation occurred on YO_x/Silicalite-1. The authors proposed that the difference in activity for the two catalysts was due to differences in the strength of interactions between Y species and the supports.

https://doi.org/10.1021/jacs.1c01315
J. Am. Chem. Soc. 2021, 143, 8352−8366

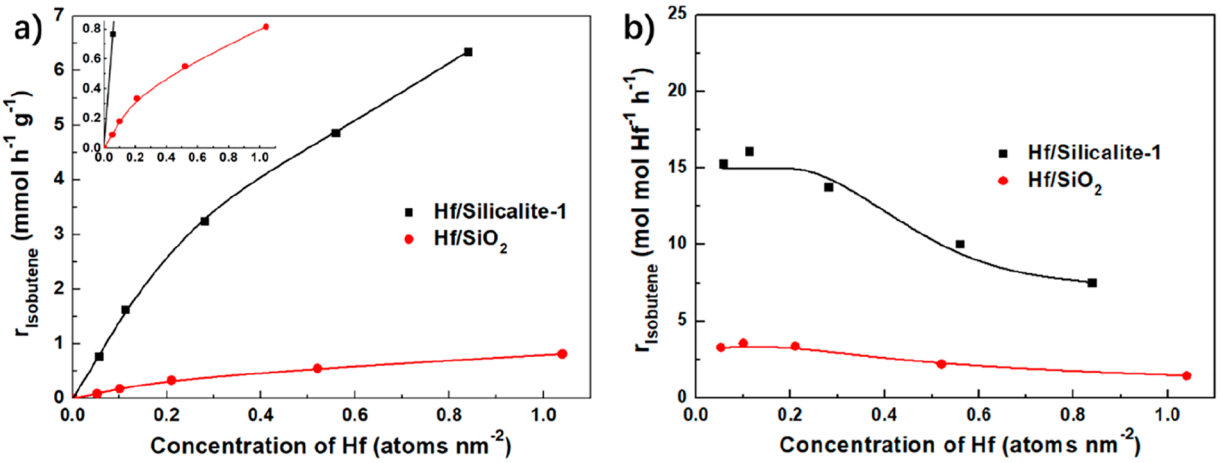

Figure 6. Rates of isobutene formation measured at 1.57 kPa acetone/He, S/C = 5, and 723 K as a function of the concentration of Hf over Hf/Silicalite-1 and Hf/SiO_2. (a) Rates normalized per catalyst mass. (b) Rates normalized per moles of Hf.

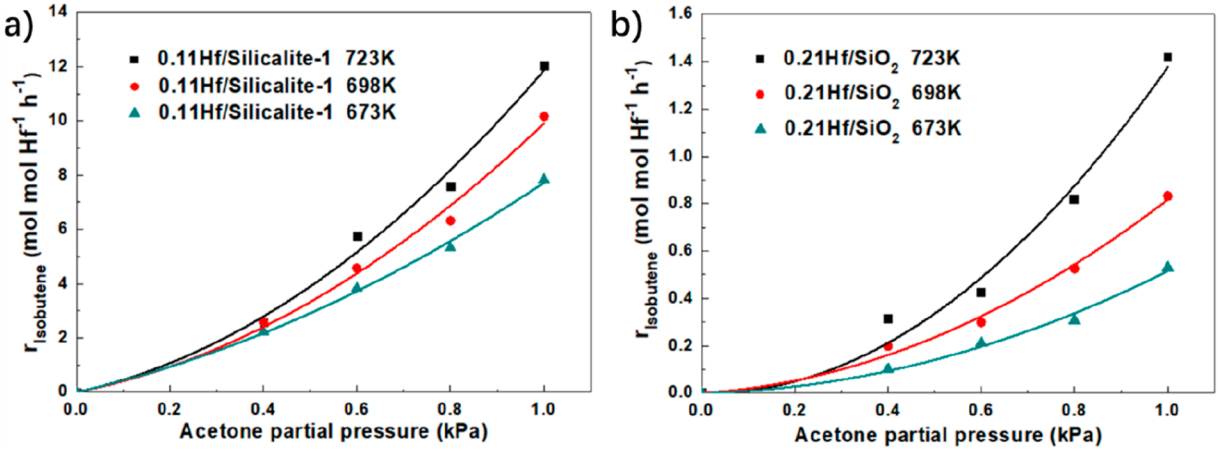

Figure 7. Dependence of the rates of isobutene formation on the acetone partial pressure measured at 673, 698, and 723 K over (a) 0.11Hf/Silicalite-1 and (b) 0.21Hf/SiO_2. Reaction conditions: catalyst mass = 20 mg for Hf/Silicalite-1 and 50 mg for Hf/SiO_2, total flow rate at STP = 20 mL/min, P_{H_2O} = 15 kPa, the S/C ratio varies between 5 and 12.5.

Figure 7 illustrates the dependence of the TOF for isobutene formation on the acetone partial pressure at different temperatures, measured under differential reaction conditions (acetone conversion <5%), for both Hf/Silicalite-1 and Hf/SiO_2. The rates of isobutene formation for both catalysts lie between second and first order in acetone partial pressure at all three temperatures (673, 698, and 723 K), suggesting that a bimolecular process is involved in the rate-limiting step.

As noted earlier, water vapor is added to the feed stream to alleviate catalyst deactivation. The effect of the water partial pressure on the TOF for isobutene formation for a fixed acetone partial pressure is shown in Figure 8. For 0.21Hf/SiO_2, the TOF for isobutene decreases by a factor of 2 as the partial pressure of water vapor is raised from 3 to 10 kPa but then remains constant for a further increase in the partial pressure of water vapor. In the case of 0.11Hf/Silicalite-1, the TOF for isobutene again decreases with increasing partial pressure but becomes constant for water vapor partial pressures above 15 kPa. However, in contrast to Hf/SiO_2, the TOF decreases by a factor of 1.5.

The influence of water partial pressure on the TOF for isobutene formation on supported Hf catalysts with different Hf loadings was studied further. As seen in Figure S7, similar

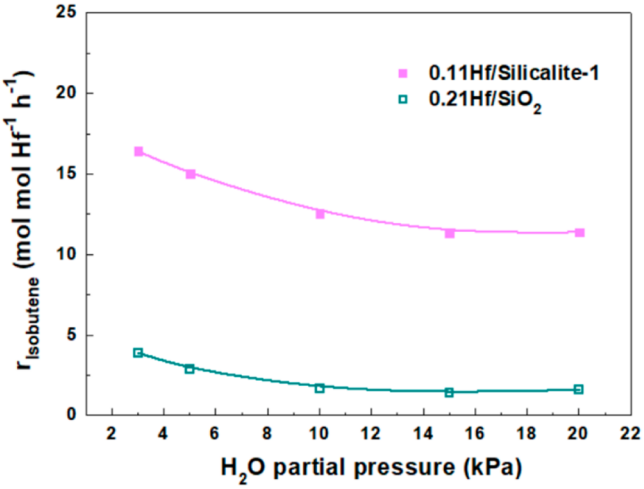

Figure 8. Influence of water partial pressure on the formation rate of isobutene from acetone on Hf/Silicalite-1 and Hf/SiO_2 catalysts. Reaction conditions: 723 K, P_A = 1 kPa, $m_{cat.}$ = 20 mg for 0.11Hf/Silicalite-1 and 50 mg for 0.21Hf/SiO_2.

https://doi.org/10.1021/jacs.1c01315
J. Am. Chem. Soc. 2021, 143, 8352−8366

effects of water partial pressure on the rates of isobutene formation are observed for all of the Hf supported catalysts. The rate of isobutene formation decreases with increasing water partial pressures and then reaches a plateau. The rate of isobutene formation decreases by 47% for 0.056Hf/Silicalite-1, 41% for 0.28Hf/Silicalite-1 and 67% for 0.10Hf/SiO_2. Despite some small difference, the inhibition of the rate of isobutene formation due to water is approximately independent of the Hf loading. Moreover, the TOF for isobutene formation is independent of water vapor pressure for catalysts with water partial pressures higher than 15 kPa, which agrees well with the results in Figure 6.

The decrease in the initial rate and the subsequent plateau in the rate of isobutene formation suggests the existence of more than one kind of Hf site. Considering the abundance of Si−OH on the surface of SiO_2 and Silicalite-1, generation of small numbers of Lewis acid Hf centers interacting with more Si−OH groups can be expected. As observed in Figure 6, the rates of isobutene formation on Hf sites H-bonded to one Si−OH group is 4.5 times higher than that for Hf sites that do not H-bond with adjacent Si−OH groups. Consequently, we propose that the rates of isobutene formation on Hf sites H-bonding with more Si−OH groups on Hf/Silicalite-1 are 5−10 times higher than those on Hf sites H-bonding with one Si−OH group. Based on this reasoning, Hf sites that are H-bonded with multiple Si−OH groups only consist of 7.9−4.1% of the total Hf sites to account for a decrease of 30% isobutene formation rate over 0.11Hf/Silicalite-1 as the water partial pressure increase from 3 to 20 kPa. A similar deduction is also made for Hf/SiO_2.

We hypothesize that such Lewis acid centers may adsorb water much more strongly than Hf sites interacting with only one adjacent Si−OH group. The results shown in Figure 8 suggest that water vapor does not inhibit that condensation of acetone to isobutene on the latter sites. For this reason, we do not consider inhibition of this reaction nor the ketonization of acetic acid, produced as a byproduct of acetone condensation, in our analysis of the reaction kinetics for acetone condensation (see below).

3.3. Conversion of Reaction Intermediates. Prior studies of acetone conversion to isobutene have proposed diacetone alcohol (DAA) and mesityl oxide (MO) as possible reaction intermediates.[15,58] It has also been reported that the acetic acid formed in one to one ratio with isobutene is converted back to acetone by ketonization. For this reason, we examined the reactions of DAA, MO, and acetic acid over Hf/SiO_2, Hf/Silicalite-1, SiO_2, and Silicalite-1. We were particularly interested in establishing whether DAA and MO are possible intermediates along the pathway from acetone to isobutene and acetic acid and whether the rate of acetic acid ketonization is faster than the rate of its formation.

Complete conversion of DAA occurs when it is fed together with water vapor over Hf/Silicalite-1 and Hf/SiO_2 at 723 K. The principal products are acetone and a small amount of isobutene. Interestingly, the distribution of products is nearly identical to that observed when the same concentration of acetone on a carbon basis was used as the reactant, in good agreement with previous studies.[5,59] The facile decomposition of DAA at 723 K to acetone is fully expected because the standard-state Gibbs free energy of reaction for this process is −118 kJ/mol, and the enthalpy of reaction is only 6.3 kJ/mol, as presented in Figures S8 and S9. Therefore, very little activation is required to promote the decomposition of DAA.

MO together with water at a S/C ratio of 5 was fed over Hf/Silicalite-1 and Hf/SiO_2 as well as the supports at 723 and 573 K. As observed in Figure 9, both Silicalite-1 and SiO_2 catalyze

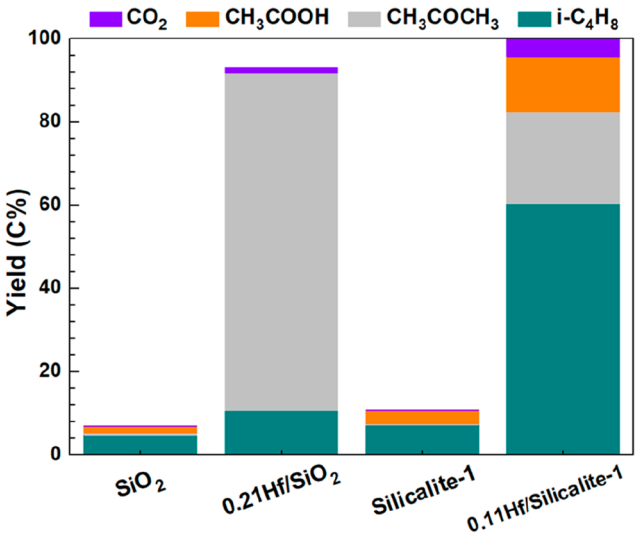

Figure 9. Product distribution of mesityl oxide conversion over SiO_2, Silicalite-1, and Hf supported samples at 723 K. Catalyst mass = 15 mg, P_{MO} = 0.49 kPa, S/C = 5, total flow rate at STP = 20 mL/min.

the conversion of MO to isobutene at 723 K with isobutene as the main product. The catalyst for these reactions is likely the mildly acidic Si−OH groups on the surface of SiO_2 and Silicalite-1. This interpretation is similar to that proposed for DeAlBEA.[15] Silicalite-1 is more active than SiO_2 due to the stronger acidity of its Si−OH groups, as suggested by the presence of H-bonded pyridine bands (1596 and 1448 cm^{-1}) (see Figure 1b).

The conversion of MO is much higher over 0.21Hf/SiO_2 (>90% at 723 K, Figure 9) than over SiO_2. Acetone is the dominant product, and the yield of isobutene is not significantly enhanced compared with that formed over SiO_2. Lowering the temperature to 573 K eliminates the formation of isobutene, and only acetone is observed (Figure S10). By contrast, much more isobutene is generated at 723 and 573 K (Figure 9 and Figure S10) over 0.11Hf/Silicalite-1 compared with Silicalite-1. Acetic acid, the byproduct of MO hydrolysis, is also observed. The formation of acetone over both catalysts can be ascribed to the hydrolysis of MO (the reverse of the reaction that forms MO by the condensation of acetone), for which the Gibbs free energy of reaction is −23.8 kJ/mol, a value that is only slightly more endergonic than that for the hydrolysis of MO to form isobutene and acetic acid, −26.5 kJ/mol (Figure S8). Therefore, we suggest that the preferential formation of acetone vs isobutene from MO over 0.21Hf/SiO_2 compared to 0.11Hf/Silicalite-1 indicates that the formation of isobutene on 0.21Hf/SiO_2 is limited kinetically. We propose that the higher isobutene selectivity of 0.11Hf/Silicalite-1 relative to 0.21Hf/SiO_2 is due to the moderate Brønsted acidity of Hf−OH groups that are H-bonded with adjacent Si−OH groups on Hf/Silicalite-1. However, this kind of Brønsted acidic sites is not strong enough to protonate pyridine as demonstrated by the absence of Brønsted acidic pyridine adsorption band at 1545 cm^{-1}. This interpretation has also been suggested in previous studies, which have shown that moderately Brønsted acidic M−OH···HO−Si sites formed on

https://doi.org/10.1021/jacs.1c01315
J. Am. Chem. Soc. 2021, 143, 8352−8366

metal-incorporated zeolites[39] are active for the hydrolysis of MO to isobutene and acetic acid.[60,61]

The reaction of acetic acid at 723 K was examined over 0.21Hf/SiO_2 and 0.11Hf/Silicalite-1 as well as over each support (Figure 10). SiO_2 and Silicalite-1 exhibit negligible activity for the conversion of acetic acid to acetone. However, both 0.11Hf/Silicalite-1 and 0.21Hf/SiO_2 exhibit significant rates of acetone formation, 3.76 and 3.18 mmol h^{-1} g^{-1}, respectively, demonstrating that Lewis acidic Hf sites are the active sites for acetic acid ketonization. Lewis acidic Zr and Y sites have also been found to be active for the ketonization of carboxylic acid.[15,19] In addition to acetone, noticeable amounts of isobutene are generated over Hf-containing catalysts. It is also noted that the rate of isobutene formation on 0.11Hf/Silicalite-1 is about 3.6 times higher than that of 0.21Hf/SiO_2, which agrees closely with the relative rates of isobutene formation observed when acetone is the reactant. It is also notable that the rates of acetic acid ketonization are 3.4 and 13.9 times the rates of isobutene formation from acetone over 0.11Hf/Silicalite-1 and 0.21Hf/SiO_2, respectively, which explains why acetic acid is not observed as a product when acetone is used as the reactant.

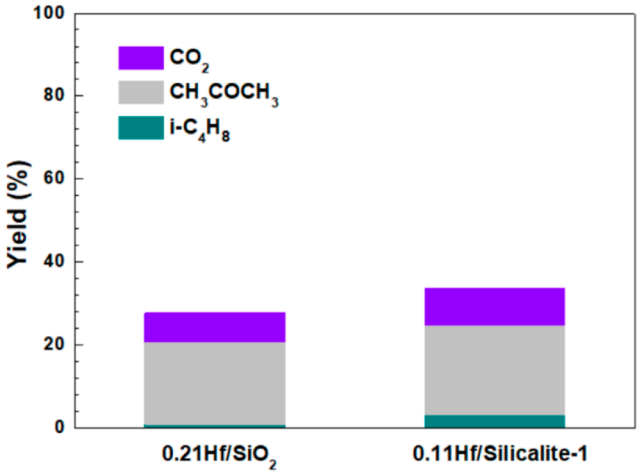

Figure 10. Products yields observed during the conversion of acetic acid over Hf/Silicalite-1 and Hf/SiO_2 at 723 K. Catalyst mass = 20 mg, P_{AA} = 0.5 kPa, STP = 40 mL/min.

3.4. IR Spectroscopy of Absorbed Species. In situ FTIR spectra of acetone and MO reacting on Hf/Silicalite-1 were acquired to gain more insight into the reaction mechanism. As shown in Figure 11a, when acetone is fed as a reactant, a strong peak is observed centered at 1690 cm^{-1} that is characteristic of the vibration of ν(C═O) in molecular acetone adsorbed on Lewis acidic Hf.[15,58] Due to the overlap of the ν(C═O) vibration in acetone, DAA, and MO, it is hard to distinguish the generation of possible C_6 intermediates using this feature. However, during the reaction of acetone, a broad peak appears at 1596 cm^{-1} and strengthens with time. This band can be ascribed to ν(C═C) stretching vibrations of MO adsorbed on Hf sites. The assignment of this band to MO is supported by its observation in the spectrum of adsorbed MO, as seen in Figure 11b.[15,58,62] Although the enol form of acetone has a structure that is similar to that of MO, the enolization of acetone and subsequent aldol condensation proceed very rapidly, making it very difficult to observe the enol form of acetone.[63] The first evidence for enolate species has recently been reported in an IR study of acetone conversion on $Zn_xZr_yO_z$. This work clearly demonstrated that the ν(C═C) infrared stretching vibration of the acetone enolate and MO are located at 1517 and 1596 cm^{-1}, respectively.[63] Building on these findings, the appearance of a band at 1596 cm^{-1} for the ν(C═C) stretching vibration together with the presence of bands at 3010 and 2920 cm^{-1} for ν(C−H) stretching vibrations evidence for the formation of MO from acetone at 306 K.[15,58,63]

3.5. Mechanism and Kinetics of Acetone Conversion to Isobutene. Scheme 2 illustrates the proposed mechanism for the conversion of acetone to isobutene and acetic acid over Hf/Silicalite-1. Reaction begins with the stepwise adsorption of two molecules of acetone onto a Lewis acidic Hf site (Steps I and II). Both forms of adsorbed acetone involve a Lewis base-acid interaction of the oxygen atom of the C═O group with the Hf cation. This form of adsorption is supported by DFT calculations for the interactions of acetone with isolated Zr species on silica (≡Zr−OH).[19] Further supporting the proposed form of acetone adsorption we note that the frequency of C═O vibrations for acetone shifts from 1740

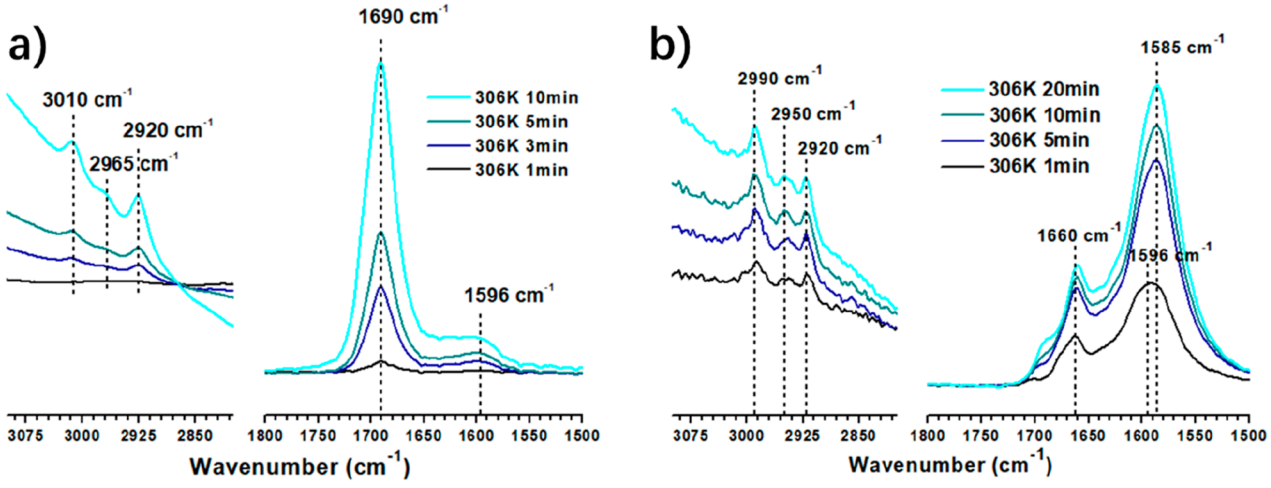

Figure 11. In situ FTIR spectra taken during the reaction of (a) acetone and (b) mesityl oxide over 0.28Hf/Silicalite-1. 2 μL of acetone or 0.2 μL of mesityl oxide was fed with He at a STP flow rate = 30 mL/min.

https://doi.org/10.1021/jacs.1c01315
J. Am. Chem. Soc. 2021, 143, 8352−8366

Scheme 2. Proposed Reaction Mechanism for Acetone Conversion to Isobutene over Hf/Silicalite-1

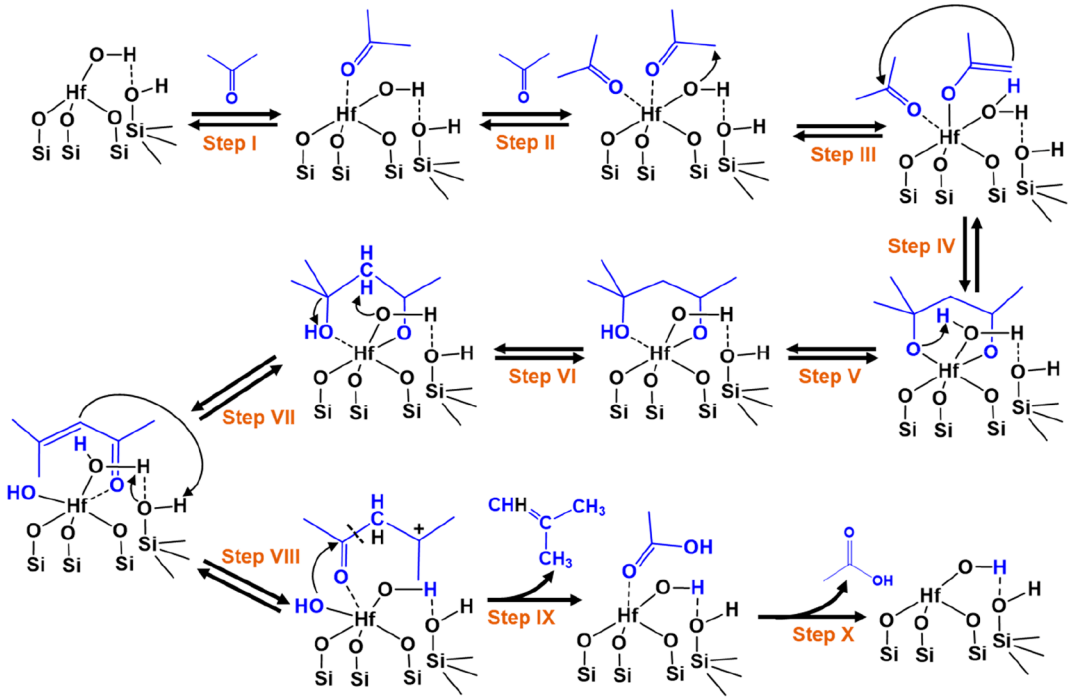

Scheme 3. Proposed Reaction Mechanism for Acetic Acid Ketonization over Hf/Silicalite-1

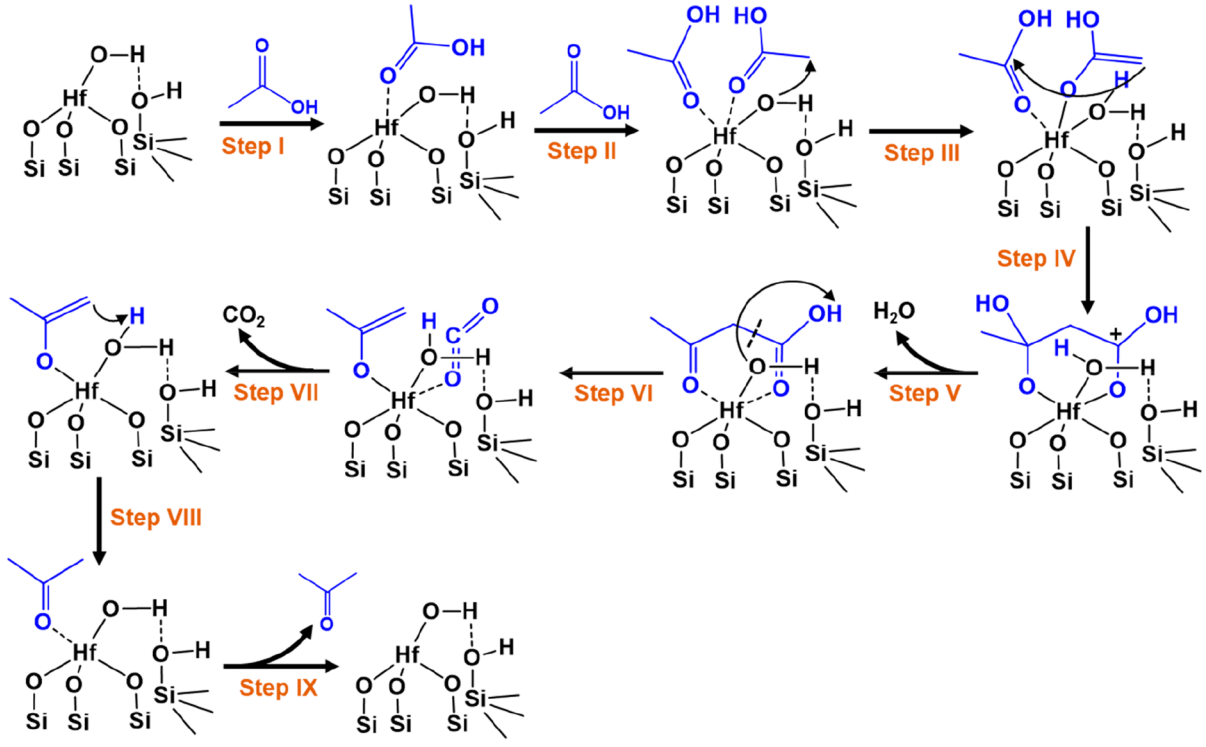

cm^{-1} in the gas phase to 1690 cm^{-1} upon absorption on Hf/Silicalite-1. The next step in the pathway (Step III) is enolization of one of the adsorbed acetone molecules, a process that involves the transfer of a proton to the Lewis basic O atom of the OH group associated with Hf (Hf−OH). This mechanism has been proposed for the aldol condensation of acetone and cross-aldol condensation of aromatic aldehydes with acetone over Lewis acidic metals supported on SiO_2, incorporated into zeolite beta, and present on the surface of $Zn_xZr_yO_z$.[18,19,63] Polarization of the C═O bond of an adsorbed acetone via interaction of the nucleophilic oxygen atom and the electrophilic Hf site acidifies the α-H on one of the methyl groups of acetone, thereby facilitating its abstraction by the basic hydroxyl oxygen on the Hf site to

https://doi.org/10.1021/jacs.1c01315
J. Am. Chem. Soc. 2021, 143, 8352−8366

form an enolate intermediate and bound H_2O. This step is then followed by nucleophilic attack of the enolate on the electrophilic carbonyl carbon of the second adsorbed acetone molecule, resulting in the formation of a C−C bond (Step IV). The bound water acts as a Brønsted acid. The aldol condensation intermediate is formed via abstraction of a proton from bound water, which rapidly dehydrates to produce thermodynamically favored MO (Step VI and VII). This proposal is verified by the presence of IR signal at 1596 cm^{-1} corresponding to C═C vibration in MO adsorbed on Hf sites during the reaction of acetone (see Figure 11a). As demonstrated experimentally, the further conversion of adsorbed MO is rapid because MO is not observed as a stable intermediate. We propose that in Step VIII protonation of the α-carbon of adsorbed MO occurs by attack of the Brønsted acid Si−OH group that is H-bonded to an adjacent Hf sites and that the hydroxyl H atom on Hf regenerates the Si−OH, resulting in the formation of a carbocation intermediate. This intermediate then undergoes C−C cleavage to produce isobutene and acetic acid with the simultaneous addition of a hydroxyl group that transfers from the Hf site to the carbonyl carbon (Step IX). The acetic acid then either desorbs or undergoes ketonization to produce acetone and CO_2. The reaction mechanism envisioned for acetone conversion to isobutene over Hf/SiO_2 is thought to be similar to that shown in Scheme 2. However, for Hf/SiO_2 (see Scheme S1), due to the absence of H-bonding between Hf−OH and an adjacent Si−OH group, the O atom of Hf−OH will be less basic and, hence, will be less favorable for the enolization step (Step III). This, in turn, will retard C−C formation and, hence, the rate of isobutene formation. In addition, the absence of H-bonding between adjacent Hf−OH and Si−OH groups makes the H of Si−OH over Hf/SiO_2 less acidic, thereby retarding protonation of the adsorbed MO carbon by comparison to what occurs on Hf/Silicalite-1.

Scheme 3 illustrates the proposed mechanism for ketonization of acetic acid over isolated Hf sites on Hf/Silicalite-1. This scheme parallels that proposed for the ketonization of propanoic acid on isolated ≡Zr−OH sites supported on silica.[19] The reaction begins with the adsorption of two acetic acid molecules through a Lewis acid−base interaction between the nucleophilic carbonyl oxygen of acetic acid and the electrophilic Hf, as presented in Steps I and II. Polarization of the carbonyl groups makes the α-H of an adsorbed acetic acid more acidic and, therefore, the basic hydroxyl oxygen in Hf−OH can abstract the α-H and form an adsorbed enolized carboxylic acid and adsorbed H_2O (Step III). Subsequent nucleophilic attack by the α-C of the enolate on to the electrophilic carbonyl carbon of the second adsorbed acetic acid leads to the formation of a carbocation intermediate, which contains a new C−C bond (Step IV). The next step is the abstraction of a proton from the water bounded to Hf sites to the hydroxyl group of this intermediate, followed by dehydration to produce an adsorbed β-keto acid (Step V). Subsequently, in Step VI, deprotonation and C−C bond cleavage of the β-keto acid intermediate leads to decarboxylation and formation of an enolized ketone species. After the desorption of CO_2, the proton abstracted from the β-keto acid intermediate is transferred to the negatively charged enolized ketone carbon, producing adsorbed acetone (Step VIII). Finally, the desorption of acetone closes the reaction cycle. Ketonization of acetic acid over Hf/SiO_2 is envisioned to occur via an identical reaction pathway and the corresponding reaction mechanism is presented in Scheme S2.

As noted above, neither MO or acetic acid are observed as reaction intermediates, suggesting that these species are rapidly consumed and, therefore, are not involved in the rate limiting step along the pathway from acetone to isobutene. More importantly, the yield of isobutene from MO is much higher than that of acetone at similar conditions (Figure 9), indicating a much higher reactivity of MO. Therefore, the rate-limiting step for the conversion of acetone to isobutene occurs prior to the formation of MO. Together with the fact that the kinetics of isobutene formation are nearly second order in acetone concentration, we propose that the rate-limiting step involves the formation of C−C bond, Step IV in Scheme 2. This conclusion is identical to that reached for the synthesis of MO from acetone over isolated ≡Zr−OH sites supported on silica.[19] The rate expression for isobutene formation in that case is given by (see the Supporting Information for a derivation):

$$r_{IB} = \frac{K_I K_{II} K_{III} k_{IV} P_{Acet.}^2}{(1 + K_I P_{Acet.} + K_I K_{II} P_{Acet.}^2)} \quad (1)$$

In eq 1, r_{IB} is the rate of isobutene formation per Hf site; K_I, K_{II}, and K_{III} are the equilibrium constants for Step I, II, and III, respectively; k_{IV} is the rate coefficient for Step IV; and $P_{Acet.}$ is the partial pressure of acetone.

Eq 1 was fit to the measured rate data by nonlinear least-squares regression. The quality of the fit is very good as can be judged by the parity plot shown in Figure S11. For both catalysts, the value of R^2 is 0.98. To further test the validity of the rate expression of isobutene formation, we measured the rates of isobutene formation at acetone partial pressure of 3 and 5 kPa at 723 K, and the results are presented in Figure S12. As shown, the rates of isobutene formation estimated by eq 1 at these conditions deviated from experimental observation by no more than 15% at 5 kPa for Hf/SiO_2, thereby further demonstrating the reliability of eq 1 and the fitted parameters.

The fitted rate parameters for Hf/SiO_2 are given in Table 1. The estimated enthalpies for adsorption of the first and second molecules of acetone (ΔH_{ads}) are −34.7 and −25 kJ/mol, respectively. These values are lower than those calculated for Zr/SiO_2 containing isolated Zr sites, for which the adsorption enthalpies for the first and second molecules of acetone are −80 and −75 kJ/mol, respectively.[19] The lower adsorption enthalpies for Hf compared to Zr is attributed to the lower Lewis acidity of Hf. Consistent with this reasoning, we note that apparent order in acetone partial pressure is close to zero

Table 1. Rate Parameters for Isobutene Formation over Hf/SiO_2

	rate parameters	K_I, kPa^{-1}	K_{II}, kPa^{-1}	$K_{III}k_{IV}$, mol mol Hf^{-1} h^{-1}
T, K	673	0.1936	0.0931	38
	698	0.1522	0.0778	76
	723	0.1262	0.0684	158
entry	first acetone molecule ΔH_{ads}, kJ/mol	−34.7		
	second acetone molecule ΔH_{ads}, kJ/mol		−25.0	
	intrinsic E_a, kJ/mol			116.3

https://doi.org/10.1021/jacs.1c01315
J. Am. Chem. Soc. 2021, 143, 8352−8366

for Zr/SiO_2[19] but nearly second order for Hf/SiO_2, as reported here. The effective activation energy under conditions of zero order dependence on acetone partial pressure on isolated Hf sites of Hf/SiO_2, calculated for $K_{III}k_{IV}$, is 116.3 kJ/mol.

The fitted rate parameters for isobutene formation over Hf/Silicalite-1 are presented in Table 2. The enthalpy of acetone

Table 2. Rate Parameters for Isobutene Formation over Hf/Silicalite-1

	rate constants	K_I, kPa^{-1}	K_{II}, kPa^{-1}	$K_{III}k_{IV}$, mol mol Hf^{-1} h^{-1}
	673	0.547	0.386	70
T, K	698	0.421	0.311	118
	723	0.3241	0.2662	187
entry	first acetone molecule ΔH_{ads}, kJ/mol	−42.3		
	second acetone molecule ΔH_{ads}, kJ/mol		−30.1	
	intrinsic E_a, kJ/mol			79.5

adsorption on Hf/Silicalite-1 is higher than that for Hf/SiO_2 due to the stronger acidity of Hf sites of Hf/Silicalite-1, consistent with the conclusion drawn from IR spectra of adsorbed pyridine. The effective activation energy, calculated for $K_{III}k_{IV}$, is 79.5 kJ/mol, which is much lower than that obtained for Hf/SiO_2 (116.3 kJ/mol). This difference is attributed to H-bonding interaction between Hf−OH and adjacent Si−OH on Hf/Silicalite-1, which strengthens the nucleophilic oxygen atom of Hf−OH, consequently facilitates α-H abstraction from adsorbed acetone, and enhances the aldol condensation of acetone.

4. CONCLUSIONS

Hf was grafted onto SiO_2 and Silicalite-1. Characterization by IR spectroscopy, ^{1}H MAS NMR, and UV−vis spectroscopy indicates that for surface concentration below 0.28 Hf atoms nm^{-2} for Hf/Silicalite-1 and 0.21 Hf atoms nm^{-2} for Hf/SiO_2, Hf is present as isolated sites bonded to the support as $(\equiv Si-O)_3-Hf-OH$ groups. In the case of Hf/Silicalite-1, the Hf−OH groups H-bond with adjacent Si−OH groups ($(\equiv Si-O)_3-Hf-OH\cdots HO-Si\equiv$). Both Hf/SiO_2 and Hf/Silicalite-1 are active for the conversion of acetone to isobutene. Despite the similarity in chemical structure, the active sites on Hf/Silicalite-1 exhibit a TOF for isobutene formation at 723 K that is 4.5 times that on Hf/SiO_2. This difference is attributed to H-bonding interaction between Hf−OH and adjacent Si−OH on Hf/Silicalite-1. Isolated Lewis acidic Hf sites are responsible for the acetone aldol condensation step to form mesityl oxide (MO), which is observed by in situ IR spectra. Studies of the reactions of potential intermediates (DAA and MO) suggest that isobutene formation occurs via the hydrolysis of MO, catalyzed by Hf sites. Hf−OH groups H-bonded with Si−OH groups on Hf/Silicalite-1 exhibits moderate Brønsted acidity and are much more effective for C−C cleavage of MO. During this process, one equivalent of acetic acid is generated per equivalent of isobutene, and the acetic acid is then rapidly converted back to acetone via ketonization on the Lewis acidic Hf sites. The rate of isobutene formation exhibits close to second order kinetics both on Hf/SiO_2 and Hf/Silicalite-1 for the range of acetone partial pressure explored, suggesting that the rate-limiting step involves C−C bond formation between two acetone molecules.

■ ASSOCIATED CONTENT

Supporting Information

The Supporting Information is available free of charge at https://pubs.acs.org/doi/10.1021/jacs.1c01315.

Supplemental catalyst characterization (XRD patterns, BET, ICP, SEM, pyridine adsorbed FTIR, ^{1}H NMR) (Figures S1−S6, Table S1−S5); theoretical deduction of the structure of isolated Hf sites based on ^{1}H NMR; supplemental reaction results (Figures S7, S10); gas-phase Gibbs free energy and enthalpy of formation (Figure S8 and S9); reaction mechanisms of acetone aldol condensation and acetic acid ketonization on Hf/SiO_2 (Schemes S1 and S2), derivation of rate expressions, and parity plots comparing the rates of isobutene formation obtained experimentally and estimated from eq 1 (Figures S11 and S12) (PDF)

■ AUTHOR INFORMATION

Corresponding Author

Alexis T. Bell − *Chemical Sciences Division, Lawrence Berkeley National Laboratory, Berkeley, California 94720, United States; Department of Chemical and Biomolecular Engineering, University of California, Berkeley, Berkeley, California 94720, United States;* orcid.org/0000-0002-5738-4645; Email: alexbell@berkeley.edu

Authors

Yanfei Zhang − *Chemical Sciences Division, Lawrence Berkeley National Laboratory, Berkeley, California 94720, United States; Department of Chemical and Biomolecular Engineering, University of California, Berkeley, Berkeley, California 94720, United States*

Liang Qi − *Chemical Sciences Division, Lawrence Berkeley National Laboratory, Berkeley, California 94720, United States; Department of Chemical and Biomolecular Engineering, University of California, Berkeley, Berkeley, California 94720, United States*

Alicia Lund − *Chemical Sciences Division, Lawrence Berkeley National Laboratory, Berkeley, California 94720, United States; Department of Chemical and Biomolecular Engineering, University of California, Berkeley, Berkeley, California 94720, United States*

Peng Lu − *Department of Chemical and Biomolecular Engineering & Institute for NanoBioTechnology, Johns Hopkins University, Baltimore, Maryland 21218, United States*

Complete contact information is available at: https://pubs.acs.org/10.1021/jacs.1c01315

Notes

The authors declare no competing financial interest.

■ ACKNOWLEDGMENTS

This work was supported by the Office of Science, Office of Basic Energy Sciences of the U.S. Department of Energy under Contract DE-AC02-05CH11231. L. Qi also acknowledges support from the Dalian Institute of Chemical Physics, Chinese Academy of Sciences, People's Republic of China.

REFERENCES

(1) Marchionna, M.; Di Girolamo, M.; Patrini, R. Light Olefins Dimerization to High Quality Gasoline Components. *Catal. Today* **2001**, *65*, 397−403.

(2) Collignon, F.; Mariani, M.; Moreno, S.; Remy, M.; Poncelet, G. Gas Phase Synthesis of MTBE from Methanol and Isobutene over Dealuminated Zeolites. *J. Catal.* **1997**, *166*, 53−66.

(3) Ancillotti, F.; Fattore, V. Oxygenate Fuels: Market Expansion and Catalytic Aspect of Synthesis. *Fuel Process. Technol.* **1998**, *57*, 163−194.

(4) Mascal, M. Chemicals from Biobutanol: Technologies and Markets. *Biofuels, Bioprod. Biorefin.* **2012**, *6*, 483−493.

(5) Rorrer, J. E.; Toste, F. D.; Bell, A. T. Mechanism and Kinetics of Isobutene Formation from Ethanol and Acetone over ZnxZryOz. *ACS Catal.* **2019**, *9*, 10588−10604.

(6) Bender, M. An Overview of Industrial Processes for the Production of Olefins−C_4 Hydrocarbons. *ChemBioEng Rev.* **2014**, *1*, 136−147.

(7) Fernández-Morales, J. M.; Castillejos, E.; Asedegbega-Nieto, E.; Dongil, A. B.; Rodríguez-Ramos, I.; Guerrero-Ruiz, A. Comparative Study of Different Acidic Surface Structures in Solid Catalysts Applied for the Isobutene Dimerization Reaction. *Nanomaterials* **2020**, *10*, 1235.

(8) Mortensen, P. M.; Grunwaldt, J.-D.; Jensen, P. A.; Knudsen, K.; Jensen, A. D. A Review of Catalytic Upgrading of Bio-Oil to Engine Fuels. *Appl. Catal., A* **2011**, *407*, 1−19.

(9) Sun, J.; Zhu, K.; Gao, F.; Wang, C.; Liu, J.; Peden, C. H.; Wang, Y. Direct Conversion of Bio-Ethanol to Isobutene on Nanosized ZnxZryOz Mixed Oxides with Balanced Acid−Base Sites. *J. Am. Chem. Soc.* **2011**, *133*, 11096−11099.

(10) Hirota, Y.; Nakano, Y.; Watanabe, K.; Uchida, Y.; Miyamoto, M.; Egashira, Y.; Nishiyama, N. Effect of Crystal Size on Acetone Conversion over SAPO-34 Crystals. *Catal. Lett.* **2012**, *142*, 464−468.

(11) Ponomareva, O. A.; Mal'tseva, A. A.; Maerle, A. A.; Rodionova, L. I.; Pavlov, V. S.; Dobryakova, I. V.; Belova, M. V.; Ivanova, I. I. Production of Isobutylene from Acetone over Micro−Mesoporous Catalysts. *Pet. Chem.* **2016**, *56*, 253−258.

(12) Herrmann, S.; Iglesia, E. Selective Conversion of Acetone to Isobutene and Acetic Acid on Aluminosilicates: Kinetic Coupling between Acid-Catalyzed and Radical-Mediated Pathways. *J. Catal.* **2018**, *360*, 66−80.

(13) Hutchings, G. J.; Johnston, P.; Lee, D. F.; Williams, C. D. Acetone Conversion to Isobutene in High Selectivity Using Zeolite β Catalyst. *Catal. Lett.* **1993**, *21*, 49−53.

(14) Kyriienko, P. I.; Larina, O. V.; Soloviev, S. O.; Orlyk, S. M.; Calers, C.; Dzwigaj, S. Ethanol Conversion into 1,3-Butadiene by the Lebedev Method over MTaSiBEA Zeolites (M = Ag, Cu, Zn). *ACS Sustainable Chem. Eng.* **2017**, *5*, 2075−2083.

(15) Yan, T.; Yang, L.; Dai, W.; Wu, G.; Guan, N.; Hunger, M.; Li, L. Cascade Conversion of Acetic Acid to Isobutene over Yttrium-Modified Siliceous Beta Zeolites. *ACS Catal.* **2019**, *9*, 9726−9738.

(16) Okumura, K.; Iwasawa, Y. Zirconium Oxides Dispersed on Silica Derived from Cp_2ZrCl_2, $[(i\text{-}PrCp)_2ZrH(\mu\text{-}H)]_2$, and $Zr(OEt)_4$ Characterized by X-Ray Absorption Fine Structure and Catalytic Ketonization of Acetic Acid. *J. Catal.* **1996**, *164*, 440−448.

(17) Hanna, D. G.; Shylesh, S.; Li, Y.-P.; Krishna, S.; Head-Gordon, M.; Bell, A. T. Experimental and Theoretical Study of n-Butanal Self-Condensation over Ti Species Supported on Silica. *ACS Catal.* **2014**, *4*, 2908−2916.

(18) Lewis, J. D.; Van de Vyver, S.; Roman-Leshkov, Y. Acid-Base Pairs in Lewis Acidic Zeolites Promote Direct Aldol Reactions by Soft Enolization. *Angew. Chem., Int. Ed.* **2015**, *54*, 9835−9838.

(19) Shylesh, S.; Bettinson, L. A.; Aljahri, A.; Head-Gordon, M.; Bell, A. T. Experimental and Computational Studies of Carbon−Carbon Bond Formation via Ketonization and Aldol Condensation over Site-Isolated Zirconium Catalysts. *ACS Catal.* **2020**, *10*, 4566−4579.

(20) Iida, T.; Ohara, K.; Roman-Leshkov, Y.; Wakihara, T. Zeolites with Isolated-framework and Oligomeric-extraframework Hafnium Species Characterized with Pair Distribution Function Analysis. *Phys. Chem. Chem. Phys.* **2018**, *20*, 7914−7919.

(21) De Baerdemaeker, T.; Feyen, M.; Müller, U.; Yilmaz, B.; Xiao, F.-S.; Zhang, W.; Yokoi, T.; Bao, X.; Gies, H.; De Vos, D. E. Bimetallic Zn and Hf on Silica Catalysts for the Conversion of Ethanol to 1,3-Butadiene. *ACS Catal.* **2015**, *5*, 3393−3397.

(22) Wang, C.; Zheng, M.; Li, X.; Li, X.; Zhang, T. Catalytic Conversion of Ethanol into Butadiene over High Performance LiZnHf-MFI Zeolite Nanosheets. *Green Chem.* **2019**, *21*, 1006−1010.

(23) Zhu, Q.; Yin, L.; Ji, K.; Li, C.; Wang, B.; Tan, T. Effect of Catalyst Structure and Acid−Base Property on the Multiproduct Upgrade of Ethanol and Acetaldehyde to C_4 (Butadiene and Butanol) over the Y−SiO_2 Catalysts. *ACS Sustainable Chem. Eng.* **2020**, *8*, 1555−1565.

(24) Zhang, X.; Liu, D.; Xu, D.; Asahina, S.; Cychosz, K. A.; Agrawal, K. V.; Al Wahedi, Y.; Bhan, A.; Al Hashimi, S.; Terasaki, O. Synthesis of Self-Pillared Zeolite Nanosheets by Repetitive Branching. *Science* **2012**, *336*, 1684−1687.

(25) Guefrachi, Y.; Sharma, G.; Xu, D.; Kumar, G.; Vinter, K. P.; Abdelrahman, O. A.; Li, X.; Alhassan, S.; Dauenhauer, P. J.; Navrotsky, A.; Zhang, W.; Tsapatsis, M. Steam-Induced Coarsening of Single-Unit-Cell MFI Zeolite Nanosheets and Its Effect on External Surface Bronsted Acid Catalysis. *Angew. Chem., Int. Ed.* **2020**, *59*, 9579−9585.

(26) Cory, D.; Ritchey, W. Suppression of Signals from the Probe in Bloch Decay Spectra. *J. Magn. Reson. (1969-1992)* **1988**, *80*, 128−132.

(27) Massiot, D.; Fayon, F.; Capron, M.; King, I.; Le Calvé, S.; Alonso, B.; Durand, J. O.; Bujoli, B.; Gan, Z.; Hoatson, G. Modelling One- and Two-Dimensional Solid-State NMR Spectra. *Magn. Reson. Chem.* **2002**, *40*, 70−76.

(28) Heitmann, G.; Dahlhoff, G.; Hölderich, W. Catalytically Active Sites for the Beckmann Rearrangement of Cyclohexanone Oxime to ε-Caprolactam. *J. Catal.* **1999**, *186*, 12−19.

(29) Lanzafame, P.; Barbera, K.; Perathoner, S.; Centi, G.; Aloise, A.; Migliori, M.; Macario, A.; Nagy, J. B.; Giordano, G. The Role of Acid Sites Induced by Defects in the Etherification of HMF on Silicalite-1 Catalysts. *J. Catal.* **2015**, *330*, 558−568.

(30) Qi, L.; Zhang, Y.; Conrad, M. A.; Russell, C.; Miller, J. T.; Bell, A. T. Ethanol Conversion to Butadiene over Isolated Zinc and Yttrium Sites Grafted onto Dealuminated Beta Zeolite. *J. Am. Chem. Soc.* **2020**, *142*, 14674−14687.

(31) Sushkevich, V. L.; Ivanova, I. I.; Tolborg, S.; Taarning, E. Meerwein−Ponndorf−Verley−Oppenauer Reaction of Crotonaldehyde with Ethanol over Zr-Containing Catalysts. *J. Catal.* **2014**, *316*, 121−129.

(32) Phadke, N. M.; Van der Mynsbrugge, J.; Mansoor, E.; Getsoian, A. B.; Head-Gordon, M.; Bell, A. T. Characterization of Isolated Ga^{3+} Cations in Ga/H-MFI Prepared by Vapor-Phase Exchange of H-MFI Zeolite with $GaCl_3$. *ACS Catal.* **2018**, *8*, 6106−6126.

(33) Jung, K. T.; Bell, A. T. An in Situ Infrared Study of Dimethyl Carbonate Synthesis from Carbon Dioxide and Methanol over Zirconia. *J. Catal.* **2001**, *204*, 339−347.

(34) Sushkevich, V. L.; Vimont, A.; Travert, A.; Ivanova, I. I. Spectroscopic Evidence for Open and Closed Lewis Acid Sites in ZrBEA Zeolites. *J. Phys. Chem. C* **2015**, *119*, 17633−17639.

(35) Boronat, M.; Concepción, P.; Corma, A.; Renz, M.; Valencia, S. Determination of the Catalytically Active Oxidation Lewis Acid Sites in Sn-beta Zeolites, and Their Optimisation by the Combination of Theoretical and Experimental Studies. *J. Catal.* **2005**, *234*, 111−118.

(36) Sushkevich, V. L.; Palagin, D.; Ivanova, I. I. With Open Arms: Open Sites of ZrBEA Zeolite Facilitate Selective Synthesis of Butadiene from Ethanol. *ACS Catal.* **2015**, *5*, 4833−4836.

(37) Tang, B.; Dai, W.; Wu, G.; Guan, N.; Li, L.; Hunger, M. Improved Postsynthesis Strategy to Sn-Beta Zeolites as Lewis Acid Catalysts for the Ring-opening Hydration of Epoxides. *ACS Catal.* **2014**, *4*, 2801−2810.

https://doi.org/10.1021/jacs.1c01315
J. Am. Chem. Soc. 2021, 143, 8352−8366

(38) Osmundsen, C. M.; Holm, M. S.; Dahl, S.; Taarning, E. Tin-Containing Silicates: Structure–Activity Relations. *Proc. R. Soc. London, Ser. A* **2012**, *468*, 2000–2016.
(39) Sushkevich, V. L.; Ivanova, I. I.; Yakimov, A. V. Revisiting Acidity of SnBEA Catalysts by Combined Application of FTIR Spectroscopy of Different Probe Molecules. *J. Phys. Chem. C* **2017**, *121*, 11437–11447.
(40) Li, Z.; Rieg, C.; Beurer, A.-K.; Benz, M.; Bender, J.; Schneck, C.; Traa, Y.; Dyballa, M.; Hunger, M. Effect of Aluminum and Sodium on the Sorption of Water and Methanol in Microporous MFI-Type Zeolites and Mesoporous SBA-15 Materials. *Adsorption* **2021**, *27*, 49–68.
(41) Jiang, Y.; Huang, J.; Dai, W.; Hunger, M. Solid-State Nuclear Magnetic Resonance Investigations of the Nature, Property, and Activity of Acid Sites on Solid Catalysts. *Solid State Nucl. Magn. Reson.* **2011**, *39*, 116–141.
(42) Omegna, A.; Vasic, M.; Anton van Bokhoven, J.; Pirngruber, G.; Prins, R. Dealumination and Realumination of Microcrystalline Zeolite Beta: an XRD, FTIR and Quantitative Multinuclear (MQ) MAS NMR Study. *Phys. Chem. Chem. Phys.* **2004**, *6*, 447–452.
(43) Grünberg, B.; Emmler, T.; Gedat, E.; Shenderovich, I.; Findenegg, G. H.; Limbach, H. H.; Buntkowsky, G. Hydrogen Bonding of Water Confined in Mesoporous Silica MCM-41 and SBA-15 Studied by ^{1}H Solid-State NMR. *Chem. - Eur. J.* **2004**, *10*, 5689–5696.
(44) Fleischer, U.; Kutzelnigg, W.; Bleiber, A.; Sauer, J. Proton NMR Chemical Shift and Intrinsic Acidity of Hydroxyl Groups. Ab Initio Calculations on Catalytically Active Sites and Gas-Phase Molecules. *J. Am. Chem. Soc.* **1993**, *115*, 7833–7838.
(45) Hunger, M.; Ernst, S.; Steuernagel, S.; Weitkamp, J. High-Field ^{1}H MAS NMR Investigations of Acidic and Non-Acidic Hydroxyl Groups in Zeolites H-Beta, H-ZSM-5, H-ZSM-58 and H-MCM-22. *Microporous Mater.* **1996**, *6*, 349–353.
(46) Nesterenko, N.; Thibault-Starzyk, F.; Montouillout, V.; Yuschenko, V.; Fernandez, C.; Gilson, J.-P.; Fajula, F.; Ivanova, I. Accessibility of the Acid Sites in Dealuminated Small-Port Mordenites Studied by FTIR of co-Adsorbed Alkylpyridines and CO. *Microporous Mesoporous Mater.* **2004**, *71*, 157–166.
(47) Long, J. W.; Chervin, C. N.; Balow, R. B.; Jeon, S.; Miller, J. B.; Helms, M. E.; Owrutsky, J. C.; Rolison, D. R.; Fears, K. P. Zirconia-Based Aerogels for Sorption and Degradation of Dimethyl Methylphosphonate. *Ind. Eng. Chem. Res.* **2020**, *59*, 19584–19592.
(48) Tang, B.; Dai, W.; Sun, X.; Wu, G.; Guan, N.; Hunger, M.; Li, L. Mesoporous Zr-Beta Zeolites Prepared by A Post-Synthetic Strategy As A Robust Lewis Acid Catalyst for the Ring-Opening Aminolysis of Epoxides. *Green Chem.* **2015**, *17*, 1744–1755.
(49) Mogilevsky, G.; Karwacki, C. J.; Peterson, G. W.; Wagner, G. W. Surface Hydroxyl Concentration on $Zr(OH)_4$ Quantified by ^{1}H MAS NMR. *Chem. Phys. Lett.* **2011**, *511*, 384–388.
(50) Hadjiivanov, K. Identification and Characterization of Surface Hydroxyl Groups by Infrared Spectroscopy. *Adv. Catal.* **2014**, *57*, 99–318.
(51) Datka, J; Kawałek, M; Gora-Marek, K Acid Properties of NaKH-ferrierites of Various Exchange Degrees Studied by IR Spectroscopy. *Appl. Catal., A* **2003**, *243* (2), 293–299.
(52) Rahman, I. A.; Padavettan, V. Synthesis of Silica Nanoparticles by Sol-Gel: Size-Dependent Properties, Surface Modification, and Applications in Silica-Polymer Nanocomposites—A Review. *J. Nanomater.* **2012**, *132424*, 1–15.
(53) Qasim, M.; Ananthaiah, J.; Dhara, S.; Paik, P.; Das, D. Synthesis and Characterization of Ultra-Fine Colloidal Silica Nanoparticles. *Adv. Sci., Eng. Med.* **2014**, *6*, 965–973.
(54) Gianotti, E.; Raimondi, M. E.; Marchese, L.; Martra, G.; Maschmeyer, T.; Seddon, J. M.; Coluccia, S. A Spectroscopic Sudy of Group IV Transition-Metal-Incorporated Direct Templated Mesoporous Catalysts. Part 2. A Comparison of Ti-, Zr- and Hf-Containing Materials. *Catal. Lett.* **2001**, *76*, 21–26.
(55) Vargas, M.; Murphy, N.; Ramana, C. Structure and Optical Properties of Nanocrystalline Hafnium Oxide Thin Films. *Opt. Mater.* **2014**, *37*, 621–628.
(56) Chen, S.-Y.; Lee, J.-F.; Cheng, S. Pinacol-Type Rearrangement Catalyzed by Zr-Incorporated SBA-15. *J. Catal.* **2010**, *270*, 196–205.
(57) Morey, M. S.; Stucky, G. D.; Schwarz, S.; Froba, M. Isomorphic Substitution and Postsynthesis Incorporation of Zirconium into MCM-48 Mesoporous Silica. *J. Phys. Chem. B* **1999**, *103*, 2037–2041.
(58) Li, H.; Sun, J.; Wang, Y. Surface Acetone Reactions on $Zn_xZr_yO_z$: A DRIFTS-MS Study. *Appl. Catal., A* **2019**, *573*, 22–31.
(59) Ho, C. R.; Zheng, S.; Shylesh, S.; Bell, A. T. The Mechanism and Kinetics of Methyl Isobutyl Ketone Synthesis from Acetone over Ion-Exchanged Hydroxyapatite. *J. Catal.* **2018**, *365*, 174–183.
(60) McAllister, S.; Bailey Jr, W. A.; Bouton, C. The Catalyzed Cleavage of Diacetone Alcohol and Other Ketols and Unsaturated Ketones. *J. Am. Chem. Soc.* **1940**, *62*, 3210–3215.
(61) Crisci, A. J.; Dou, H.; Prasomsri, T.; Román-Leshkov, Y. Cascade Reactions for the Continuous and Selective Production of Isobutene from Bioderived Acetic Acid Over Zinc-Zirconia Catalysts. *ACS Catal.* **2014**, *4*, 4196–4200.
(62) Panov, A.; Fripiat, J. Acetone Condensation Reaction on Acid Catalysts. *J. Catal.* **1998**, *178*, 188–197.
(63) Li, H.; Sun, J.; Li, G.; Wu, D.; Wang, Y. Real-time Monitoring of Surface Acetone Enolization and Aldolization. *Catal. Sci. Technol.* **2020**, *10* (4), 935–939.

https://doi.org/10.1021/jacs.1c01315
J. Am. Chem. Soc. 2021, 143, 8352–8366